Universidade de Aveiro Departamento de Engenharia de Materiais e Cerâmica

Ano 2017

David João Loureiro Ramada

Development and Characterization of Apatitic and Brushitic Microneedles for the Controlled Release of Antibiotics

Desenvolvimento e Caracterização de Microagulhas Apatíticas e Bruchíticas para a Libertação Controlada de Antibióticos

Universidade de Aveiro
Ano 2017

Departamento de Engenharia de Materiais e Cerâmica

David João Loureiro Ramada

Development and Characterization of Apatitic and Brushitic Microneedles for the Controlled Release of Antibiotics

Desenvolvimento e Caracterização de Microagulhas Apatíticas e Bruhíticas para a Libertação Controlada de Antibióticos

Dissertação apresentada à Universidade de Aveiro para cumprimento dos requisitos necessários à obtenção do grau de Mestre em Materiais e Dispositivos Biomédicos, realizada sob a orientação científica da Doutora Susana Maria Henriques Olhero, Investigadora no Departamento de Engenharia de Materiais e Cerâmica/CICECO-Instituto de Materiais de Aveiro, da Doutora Paula Maria da Costa Torres, Investigadora de Pós-Doutoramento no Departamento de Engenharia de Materiais e Cerâmica/CICECO-Instituto de Materiais de Aveiro da Universidade de Aveiro e da Professora Doutora Ana Francisca Bettencourt, Professora na Faculdade de Farmácia da Universidade Nova de Lisboa.

Aos meus pais pelo incansável apoio e dedicação, sem eles nada disto seria possível.

o júri

presidente	Prof. Doutora Maria Elisabete Jorge Vieira da Costa professora auxiliar da Universidade de Aveiro
	Prof. Doutor Francisco Manuel Lemos Amado professor associado com agregação da Universidade de Aveiro
	Doutora Susana Maria Henriques Olhero equiparada a investigadora auxiliar da Universidade de Aveiro

agradecimentos

Em primeiro lugar, agradecer a todos os que tornaram possível chegar a este ponto, que fizeram com que este trabalho fosse exequível.

Às minhas orientadoras, Doutora Susana Maria Henriques Olhero, Doutora Paula Maria da Costa Torres e Professora Doutora Ana Francisca Bettencourt, pela incessável paciência, compreensão e apoio, pelas horas de trabalho e disponibilidade, pela amizade dentro e fora do laboratório e por me receberem sempre de braços e coração aberto. Sem vocês, nada disto seria possível.

Aos técnicos do DeMAC/CICECO, pela disponibilidade e ajuda prestada, sempre com um sorriso. Aos meus colegas, dentro e fora do laboratório, pela força e amizade.

E, por fim, um agradecimento aos meus pais, Júlio Ramada e Helena Ramada, pelo enorme sacrifício, apoio, compreensão e amor que me permitiram terminar mais uma etapa da minha vida.

palavras-chave

Microagulhas, cimentos de fosfato de cálcio, libertação controlada de fármacos, α-TCP, β-TCP, Levofloxacina

resumo

As microagulhas (MN) são microcomponentes inovadores na entrega de fármacos via transdérmica de forma quase impercetível para o paciente. De metais a polímeros, as MN têm sido fabricadas com uma grande variedade de materiais, embora com algumas restrições quanto à resistência mecânica (limitações relacionadas com a perfuração da pele), armazenamento e altos custos de fabrico.

Na presente tese, foram utilizados cimentos à base de fosfato tricálcico (TCP) para o fabrico de MN brushíticas e apatíticas via micromoldagem. Foram sintetizados dois pós, β-TCP e BTCP (bifásico, β-TCP + α-TCP). Partindo destes pós, foram preparadas pastas cimentícias na ausência e na presença de fármaco, variando a razão líquido/pó e caracterizadas em termos de tempos de presa inicial e final, parâmetros importantes para o enchimento e desmoldagem dos componentes. Os cimentos resultantes foram caracterizados em termos de porosidade, fases cristalinas, resistência mecânica, microestrutura da superfície e metodologia de secagem. As formulações de cimento que apresentaram os resultados mais promissores para o fabrico de MN foram utilizadas para estudar a taxa de libertação do fármaco. Uma solução aquosa de ácido cítrico com concentração adequada como líquido de presa revelou ser a mais adequada. O antibiótico levofloxacina (LEV) foi utilizado como fármaco modelo.

Os resultados obtidos mostraram que a adição de LEV aumenta os tempos de presa iniciais e finais das pastas cimentícias e diminui as propriedades mecânicas dos cimentos. Uma libertação de fármaco de 100% foi alcançada para todas as formulações de cimento testadas após 48 horas de imersão. Do estudo cinético da libertação de fármaco verificou-se que o "*Coupled Mechanism"* foi o que melhor descreveu o mecanismo de libertação da LEV em todas as formulações de cimentos testadas. Com as pastas cimentícias foi possível obter microagulhas afiadas por enchimento de micromoldes e devidamente desmoldadas. Através da avaliação da sua resistência mecânica é possível prever que as MN obtidas apresentam estrutura e propriedades mecânicas adequadas para a perfuração da pele, uma vez que, é conhecido da literatura que a força necessária para que as agulhas perfurarem a pele humana é à volta de 1-5 N. Das várias agulhas testadas, os valores da força necessária para quebrar a ponta situam-se num intervalo de 57 a 110 N.

As MN à base de cimentos de TCP apresentam características adequadas para serem utilizadas como meio de administração de fármacos via transdérmica com futuro em diversas aplicações médicas. O processo de produção utilizado traz imensas vantagens quando comparado com os métodos atuais para a produção de microcomponentes, sendo simples, económico e replicável.

keywords

Microneedles, calcium phosphate cements, controlled drug release, α-TCP, β-TCP, Levofloxacin

abstract

Microneedles (MN) are an up and coming technology offering almost inconspicuous transdermal drug delivery system. From metals to polymers, microneedles have been fabricated with a high variety of materials, although with some constraints regarding mechanical strength (limitations related to skin perforation), storage and high manufacturing costs.

In the present thesis, self-setting bioceramics were used to fabricate brushitic and apatitic MN by micro-molding casting. Two precursor powders were synthesized to obtain β-TCP and BTCP (biphasic, β-TCP+α-TCP) as main phases. Cement pastes were prepared in absence and in presence of drug, varying liquid to powder ratio and characterized in terms of initial and final setting times, important parameters for casting and de-molding procedures. The resulting cements were characterized for their porosity, crystalline phases, mechanical strength, surface morphology and drying methodology. The cement formulations that presented the most promising results for MN fabrication (flowability during casting and adequate mechanical properties for de-molding without damage) were used to study drug release rate. A citric acid solution with adequate concentration was the most suitable as setting liquid in both MN types. The antibiotic levofloxacin was used as a model drug.

The results show that the addition of levofloxacin increases the setting times of the cement pastes and decreases the mechanical properties of the cements. A 100% drug release was achieved for all the tested cement formulations after 48 hours of immersion time. The drug release kinetics were evaluated being determined that the "coupled mechanism" is the one that best described the release mechanism of cements obtained from both powders. Sharp MN were successfully casted and de-molded. MN tip obtained in this work present adequate mechanical properties for skin perforation without breakage, since according to literature the insertion forces necessary for perforate human skin is around 1-5 N. Among all tested MN, the force necessary to break the tip is in the range 57 to 110 N.

From the evaluated work, calcium phosphate cement based MN present adequate characteristics to be used as a promising drug delivery microcomponent for biomedical applications. The fabrication process used (micromolding) has several advantages when compared to the current production MN processes being simple, cost-effective and replicable.

Index

Figure Index

Table index

Abbreviations and acronyms index

CaPs: Calcium Phosphates

CDHA: Calcium deficient hydroxyapatite

CPCs: Calcium Phosphate Cements

DCPD: Dicalciumphosphate dihidrate

EGC: Epoxy Gel Casting

ER: Epoxy Resins

FST: Final Setting Time

HA: Hydroxyapatite

IST: Initial Setting Time

L/P: Liquid-to-Powder Ratio

MCPA: Monocalciumphosphate anhydrous

MCPM: Monocalciumphosphate monohydrate

MIP: Mercury Intrusion Porosimetry

MN: Microneedles

npMNAs: Nanoporous Microneedle Arrays

OCE: Optical Coherence Elastography

OCT: Optical Coherence Tomography

PDMS: Polydimethylsiloxane

PMVA/MA: Poly(methylvinylether-co-maleic ahydride)

SC: Stratum Corneum

TDDS: Transdermal Drug Delivery Systems

TPM: Thermoporosimetry

α-TCP: α-tricalcium phosphate

β-TCP: β-tricalcium phosphate

Background and context

Ever since man discovered ways to treat illness in its many forms. The way how such treatments are applied is of major importance and directly affects the body's response, either positively or negatively. As so, the interest in discovering new ways to deliver chemicals as grown alongside the advances in drug discovery. The effectiveness of a drug and how it behaves in the body is directly related to the way it is delivered.

Traditionally, medicines (meaning drugs) are delivered to the body via one of two major forms: orally, with pills and syrups, and directly in the bloodstream, via hypodermic needles [1]. When using the oral method, drugs must pass through the digestive system, which can lead to a change in the drug's composition (or even loss) due to the gastric juices and metabolization by the liver [2]. During the delivery and diffusion process drug integrity must be guaranteed, as well as, it side effects that can affect the digestive system and it behavior in such environment [2].

The use of hypodermic needles (being subcutaneous, intravenous, intramuscular or intradermal) eliminate such problems, bypassing completely the digestive system, delivering the drug directly to the bloodstream. When choosing this delivery method several factors should be considered such as, the emotional trauma and pain associated with injections, the risk of needle-related injuries, patient compliance and even the safe disposal of the needles [3]. In addition, the administration of the injection requires special training and expertise.

Transdermal drug delivery (Transdermal Drug Delivery System, TDDS), a topic that as gain a lot of attention in the past years, appears as a valid alternative to the traditional methods, providing control over the rate of drug release. TDDS is a system that can provide what the other two methods cannot: it bypasses the digestive system and it does not have the same disadvantages of hypodermic injections. Besides, the skin contains a large number of antigen-presenting cells (i.e., Langerhans cells and dermal dendritic cells), becoming a suitable way for drug delivery [6-8]. Drug patches and microneedles (MN) have been both thoroughly investigated [2, 3]. The first transdermal system for systemic delivery was approved for use in the United States in 1979, a three-day patch that delivers scopolamine to treat motion sickness [7]. Ten years later, nicotine patches become the first transdermal blockbuster, raising awareness to the transdermal delivery in medicine and for the general public [4, 5]. The main difference between the two types of transdermal delivery systems is that patches are limited to a restrict amount and nature of drugs, while MN are compatible with a wide range of drugs being also more efficient in the delivery process [1]. Instead of relying on skin permeability, MNs physically introduce the drug into the body, accessing the epidermal and the top of the dermal layer of the skin. This is of major importance, as it means that the microneedles are short enough to avoid the nerve endings, causing no pain. The dimensions of MNs are lower than 1500 micrometer in length and, in the range of 50-250 and 10-25 micrometers in width and tip diameter, respectively.

Besides the above mentioned, MNs provide a number of other advantages: (i) lower concentrations can be used since the drug release is controlled, providing a precise dosage; (ii) it's a method that requires no special qualifications for administration, opening the way to auto-administration; (iii) due to its micrometric size, can be produced in large quantities, reducing the manufacturing cost and; (iv) provides total release of the drug maintaining its stability, among others [9, 10].

Three major types of MN are commonly described in the literature, depending on the drug and application: solid (which include coated and dissolving microneedles), hollow and porous [10]. Besides that, MN based material has also a significant influence on their effectiveness. Several materials are already used to produce MNs, including biodegradable polymers [11], metals [12], soluble sugars [13], glasses and ceramics [14]. Polymeric MN are easily shaped but have a low mechanical strength [4], whereas metallic MN have a high production cost and could have compatibility issues with the drug. Therefore, finding a material that can be tailored to better suit the desired characteristics and properties while reducing production cost, is still required.

Ceramic materials appear as a new alternative to the existing options. Properties such as high mechanical strength, biocompatibility, and reusability (ceramic materials can sustain high temperatures without deformation, so sterilization is a viable option) are of interest and draw increasing attention to the use of ceramic materials in the production of MNs. Research conducted by Luttge et al. showed promising results in the development of ceramic nanoporous microneedle arrays (npMNAs) for the controlled release of drugs and vaccines [4]. In this study, alumina based npMNAs have been prepared by micromolding followed by sintering at 1500 ºC [15] to create nanoporosity. The authors showed that drug nanoparticles up to 100 nm can be loaded into the npMNAs and released with success in 30 minutes upon incubation in PBS [4]. Since drug loading in npMNAs is evaluated after sintering, the amount of drug absorbed is dependent on the pore size and pore size distribution and surface absorption capacity of the npMNAs.

Finding a manufacturing process where the drug could be added during casting process could be highly advantageous.

In fact, ceramic-based components are commonly submitted to a sintering step, where the material is thermal treated at high temperatures (≥1000ºC), to create a mechanically strong solid. Besides increasing the manufacturing costs, sintering step avoids the incorporation of pharmaceuticals during processing, since drug molecules cannot withstand such high temperatures. To overcome this, the sintering step must be eliminated in order to fabricate ceramic materials capable of incorporating pharmaceuticals, while retaining its mechanical strength and drug delivery capabilities. In a recent study evaluated by B.Cai et al. [16], self-setting bioceramics were introduced as an alternative to the above ceramics. By eliminating the sintering step, the damage caused to the loaded drugs by the high temperatures was avoided, while maintaining the required mechanical strength in order to pierce skin. Brushitic microneedles loaded with Zolpidem tartrate to treat insomnia were successfully prepared by micromolding. Being a first-of-its-kind essay involving self-setting ceramic microneedles as a vehicle for controlled drug delivery, this study opens new opportunities for advacing with research in self-setting MN. Although being an innovative work, several questions need to be answered in what concerns manufacturing costs, formulations and real world day-to-day viability.

Thus, the present work will try and shed some light on the subject, exploring the production and characterization of apatitic and brushitic calcium phosphate porous microneedles and how they behave as a controlled delivery system of an antibiotic (levofloxacin).

Chapter One:

Theoretical Introduction

1. Theoretical Introduction

1.1 - The skin

The human body is a complex system composed of different organs and systems. The human skin is the largest organ of the integumentary system (organ system composed by the skin, hair and nails) composed of up to seven layers of ectodermal tissue that guards the underlying bones, ligaments, muscles and internal organs, as well as, several structures called appendages (hair follicles and glands). Surrounding all the human body, the skin is the interface with this environment, playing an important role in immunity and protecting the body against pathogens and excessive water loss. Other functions include insulation, temperature regulation, sensation, synthesis of vitamin D and regeneration. This system can be divided into two types of skin: hairy skin (with hair follicles and sebaceous glands) and glabrous skin (a skin type on the palms and soles and lacks hair follicles).

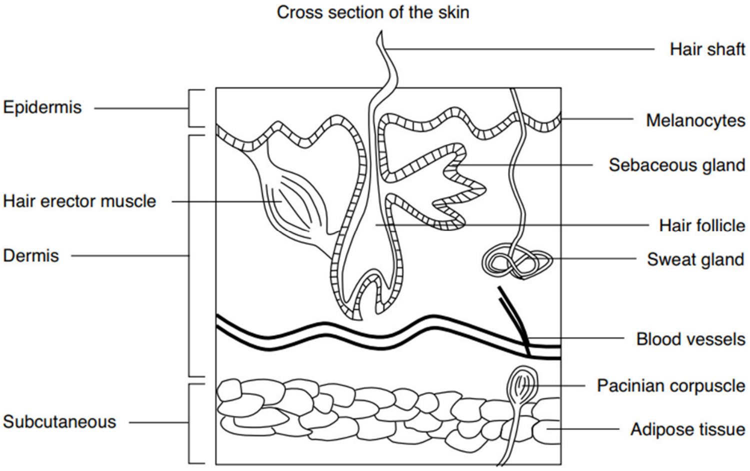

Figure 1- Cross-section of the skin, showing it 3 main layers, as well as, some of its constituents.

1.1.1 - Structure of the skin

Three layers of the skin can be recognized: epidermis, dermis and hypodermis, as illustrated in Figure 1. A healthy interaction between the layers is important for the maintenance of homeostasis in the adult. In this section, each layer will be considered separately.

Epidermis

The epidermis is the outer most layer of the skin (50 to 100 µm) that is divided into the following sublayers (Figure 2), from top to bottom [17]:

Stratum corneum (SC): consisting of mainly keratinocytes (approximately 90-95% of epidermal cells) containing a protein known as keratin. The thick layer (10 to 20 µm thick) provides a major barrier against water loss and permeation of environmental substances, as well as contributing to mechanical protection;

Stratum lucidum: this sublayer is present in the thick skin of palms and soles and consists of a thick layer of dead cells, functioning as a barrier and having water proof properties;

Stratum granulosum: also known as the granular layer, mainly consists of stratified cells arranged in one to three rows. Besides the palms and soles, the skin lacks a well-defined stratum lucidum and stratum granulosum;

Stratum spinosum: formed by cuboidal cells arranged in multiple layers, it has the capability to synthesize keratin;

Stratum basale or *Stratum germinatum*: this sublayer consists of tall columnar cells that are constantly undergoing cell division and help form new keratinocytes that will replace the dead ones form the stratum corneum.

This outmost layer of the skin contains no blood vessels, so cell nutrition is made almost exclusively by diffused oxygen from the surrounding air and, to a slighter degree, by blood capillaries extending to the outer layer of the dermis. Merkel cells and keratinocytes are the main type of cells which make up the Epidermis, with melanocytes (pigment producing cells) and Langerhans cells (dendritic immune cells) also presented [18].

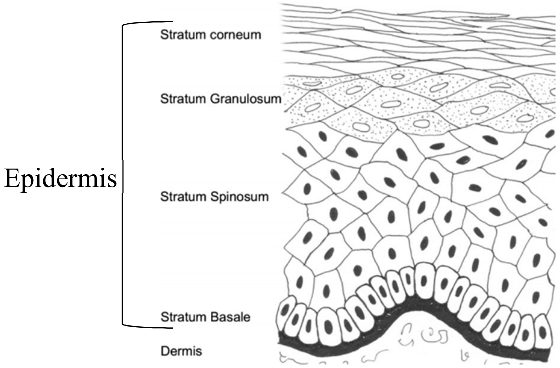

Figure 2- Diagram of the epidermis. From: (R. Randall Wickett and Marty O. Visscher) [18].

Dermis

The dermis or corium is a thick layer of skin (1 to 2 mm) that lies between the epidermis and subcutaneous layer, sustaining and supporting the epidermis. It is composed of two sublayers, the more superficial papillary dermis and the deeper reticular dermis. The papillary dermis consists of loose connective tissue containing capillaries, elastic fibers, reticular fibers and some collagen. The reticular dermis consists of a thicker layer of dense connective tissue containing larger blood vessels, closely interlaced elastic fibers and bundles of collagen fibers arranged in layers parallel to the surface. The deep surface of the dermis is highly irregular and borders the subcutaneous layer, which additionally cushions the skin [19].

Hypodermis

Also known as the subcutaneous tissue, this layer lies below the dermis and serving as a connection to the underlying bone and muscle, supplies the upper layers with blood vessels and nerves and insulates the body. Consists mainly of loose connective tissue and elastin, allowing for its mobility over underlying structures [17].

1.1.2 - Permeability of the skin

A variety of different compounds gets into contact with the skin every day, through the use of household chemicals, application of cosmetics or pharmaceutical products or even by accident. Some of those chemicals may be absorbed or facilitate the absorption of other kinds of harmful components.

The stratum corneum (SC), being the outmost layer of the epidermis, acts like a barrier preventing the penetration of molecules to the lower layers [18]. The SC is often compared to a brick wall [20], where the corneocytes (keratinocytes) are like the “bricks” and the layers of lipids between the cells like the “mortar”. This lipidic “mortar” layer is released by the keratinocytes, filling the gaps between them and preventing water from passing through. The very specialized “bricks and mortar”, work together to produce a layer that is both flexible and protective [21, 22]. Some molecules, like lipid soluble molecules, are able to diffuse through the lipid “mortar”, bypassing the barrier, but that’s not the case for all molecules. Delivery of a drug or a cosmetic into and through the skin involves a number of steps including release from the vehicle, partition into the skin and subsequent movement through the SC [23]. A complete agreement still does not exist on whether lipid layers or corneocytes are the main contributor to the permeability barrier [24]. Penetration studies and mathematical models [24-29] have demonstrated that the SC behaves like a passive diffusion barrier, being necessary additional chemicals to facilitate the diffusion though this layer, as the diffusion rate is highly dependent on the molecular weight and lipophilicity of the molecules [25]. Alternatively, mechanical penetration of the upper layer of the skin bypasses this problem. However other different problems arise related to the vehicle of delivery, its resistance, composition, biocompatibility, and general discomfort related to the application.

1.1.3 - Mechanical properties of the skin

The mechanical and biomechanical properties of the skin are of extremely importance to its health and disease, structural integrity, and aging. Studies about this subject began in the 19th century [30], further underlying its importance. Investigations in the fields of plastic surgery [31-33], skin cancer [34-36], cosmetics [37-39] and skin aging [40,41] further contributed to the understanding of the biomechanical properties of the skin.

Optical coherence electrography (OCE), also known as Optical coherence tomography (OCT) has been used to deduce mechanical properties in tissues [42, 43]. Introduced by Schmitt in 1944 [44], this technique was first used to assess the tissue biomechanics through the measurement of localized deformation and strain inside a sample. Further advances [45-48] enabled OCE to assess and extract different parameters of the tissue deformation with high accuracy and to reconstruct the tissue's biomechanical properties [49]. In a study evaluated by Xing Liang and Boppart, OCE was used to determine the mechanical properties of the skin under different conditions (normal, hydrated and dehydrated), revealing that the stratum corneum has a Young modulus of 101.20 kPa for normal skin, 21.01 kPa for hydrated skin and 300.41 kPa for dehydrated skin, confirming that the mechanical strength of the skin is directly correlated to its hydration [31].

1.1.4 - Skin Penetration

Knowing the mechanical properties of the skin is of the upmost importance when drug delivery is done through the skin. As mentioned above, the stratum corneum acts as a barrier that needs to be penetrated to efficiently deliver pharmaceuticals to the bloodstream. Structures like microneedle arrays, made from different materials, can be used to pierce the skin effectively [50]. The force needed to achieve this is a subject that has been investigated [51], being a parameter that not only affects the penetration depth but also the force that an array can handle.

In the study presented by Ryan F. Donnelly et al. [52], OCT was used for the first time to investigate the effect of a microneedle (MN) geometry and applied force upon penetration into neonatal porcine skin *in vitro* using poly(methylvinylether-co-maleic anhydride) (PMVE/MA) MNs. The research work shows that MN height can influence the extent of drug delivery across the skin and that higher application force corresponds to a higher penetration depth, as expected.

Romgens et al [53] monitored both the penetration depth and force of single solid microneedles with various tip diameters. The authors shown that sharp microneedles are essential to insert them in a well-controlled way to a desired depth.

Shape, geometry, tip diameter, mechanical strength and based materials are all parameters that need to be considered in order to create a device that can easily deliver pharmaceuticals through the skin. Microneedles appear as a suitable solution for transdermal drug delivery [9, 54-56], as discussed in the next section.

1.2 - Microneedles

For many years, hypodermic needles have been the most used technique for transdermal drug delivery. However, recent discoveries and advances in the biotechnology field showed that this delivery system has several limitations and disadvantages [11, 16]. As soon as new ways to fabricate microneedles for transporting nano-size molecules are discovered, the use of hypodermic needles could be discarded for certain applications, since they cause discomfort and limit the range of delivery.

Microneedles can be divided in three categories: solid microneedles, hollow microneedles and porous microneedles, as schematically shown in Figure 3. In turn, solid microneedles include: (i) the ones used to create porosity in the skin prior to drug administration, (ii) drug-coated solid microneedles where the drug is dissolved by the skin and the MN patch subsequently removed, and (iii) dissolving MN where complete patch containing drug molecules is adsorbed by the sky. Hollow Microneedles are considered the most challenging ones in terms of fabrication, due to the presence of a fine hole (50-100 µm) in their middle, and can be used to deliver liquid-like drugs. In porous MN, drug is usually captured in the pores and released by diffusion mechanisms after skin penetration [10].

This work, will be essentially focused on porous microneedles, its composition, geometries, fabrication methods and applications.

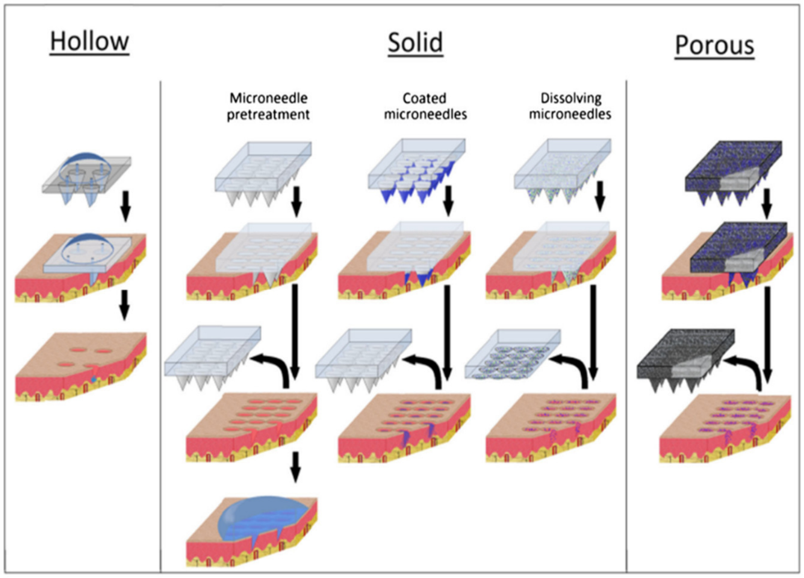

Figure 3- Different types of microneedles according to their structure and drug delivery mechanisms [4].

1.2.1 - Solid microneedles

1.2.1.1 - Materials used in the fabrication of solid microneedles

One of the first strategies for the transdermal drug delivery is based on the use of solid MNs, where the microneedle array is first applied to the skin, creating micro-channels that allow the subsequently application of the drug [10]. However, some limitations of this method are clear: (1) a two-step process is needed, which may lead to practicality issues to the end user, (2) limited to certain type of drugs (usually cosmetics), between others.

Several materials have been used to produce MNs capable of transdermal drug delivery. Considering solid MNs, silicon [58], metals, polymers [59] and ceramics [19, 20] have been used as based materials. While being a high throughput manufacturing method, microfabrication methods for most of the MNs (silicon, metals, polymers based) are often expensive, highly specialized and include complex multi-step processes [11, 21]. Standard metals usually utilized in the medical practice, such as stainless steel and titanium, have also been used as structural materials for solid MN fabrication [22-25], mainly because such materials should not raise any issues of safety, facilitating the regulatory pathway to commercial acceptance. Polymers are a viable alternative when compared to metals or silicon, although mechanical properties are usually poor.

Developing a complex structure in the micrometer scale such as a microneedle array is not an easy task. Furthermore, obtaining MN patches at an affordable cost implies the use of cost-efficient manufacturing processes. Among the high tech processes used in microneedle manufacture, such as, laser cutting [66], lithography [67] and wet and dry etching [68], micro molding is the most explored one for MN fabrication [69]. However, as in all replication methods, the first and most crucial step is to create a master structure, to obtain the mold (usually PDMS, polydimethylsiloxane, based) where the desired structure will be shaped. Although the requirements for the master structure differ with respect to the physical parameters of the chosen replication method, four basic statements are common [69]:

(a) The geometrical replication result can only be as good (or as bad) as the geometrical accuracy of the master;
(b) For the ability to separate mold and molded part (demolding step), no undercuts in the structure itself can be allowed;
(c) The surface roughness of the master should be as low as possible;
(d) A suitable interface chemistry between master and substrate must be chosen.

The prevailing technique used for fabricating PDMS devices involves master creation by a process called photolithography [70], which is a time consuming, multi-step and expensive process that needs to be carried out in a clean environment. While mold replication from the master could be an easy and costly efficient process, master fabrication involves the use of expensive advanced processing technologies. Eliminating the need for a master in micro molding fabrication could steeply decrease the total cost of the fabrication process, as well as its complexity. Hamsapriya et al. [71] published a study reporting the use of laser pulses to directly fabricate 2D and 3D structures in micro-scale on PDMS. Using a short pulse-to-pulse laser capable of achieving localized rapid heating (femtosecond laser) directly on thin PDMS layer, Hamsapriya et al. created a single-step masterless fabrication of PDMS microstructures.

Taking advantage of casting techniques in PDMS micro molding, ceramics have been recently explored for MN fabrication [15, 60, 61, 72]. Gel casting was mentioned in literature as a capable technique to fabricate this kind of micro components with complex geometries and dimensions lower that 1 mm [26, 27]. For that, ceramic suspensions parameters, such as solids loading, pH [74], surface chemistry [75] and interactions between ceramic particles with the dispersing agent [76] are of major importance and need to be precisely controlled in order to obtain the desired MN properties [60]. While in gel casting process of macro components, different gelling agents can be used, for micro component fabrication specific requirements should be addressed. The system "epoxy resin plus hardener", presented by Olhero et al. [60], has been proved to be adequate to obtain low viscosity suspensions during mold casting, to guarantee complete filling of the microparts, as well as high green strength (around 35 MPa) to de-mold them without damaging. Olhero et al.[60], highlighted for the first time, the relevance of the specific interactions between processing additives and oxide particles having different surface chemistries (alumina, silica and zirconia) in determining the kinetics of curing and the properties of green bodies consolidated by Epoxy Gel Casting (EGC) process. The work developed by Olhero et al. demonstrated that EGC is a promising technology for the microfabrication of ceramic components with complex shapes and sharp features, opening a new way for fast replicating and cost-efficient production of MN. Since ceramic MN obtained by this method should be sintered after de-molding, EGC was considered a promising technique for fabrication hollow ceramic microneedles for drugs administration in liquid form.

1.2.1.2 - Self setting ceramic MN

Even if ceramics could have some advantages when compared to polymers for MN applications, sintering procedure make them less attractive, not only due to the increase of manufacturing costs but also to the limitation in drugs incorporation before this step. To overcome this restriction, self-setting ceramics appear as alternative materials. Developing solid MNs from calcium phosphate based cements is a new research field, with only one paper published about the subject till date [16] (from author knowledge). In this study, Bing Cai et al. [16] explored the use of self-setting bioceramics for drug delivery, using Zolpidem tartrate as a model drug. Self-setting microneedles were fabricated from calcium phosphate based cements under ambient conditions to minimize drug degradation during fabrication and to facilitate a higher drug loading capacity. The drug release study showed that the release rate from this type of MN array could be controlled by the bulk surface area, porosity and resorption rate of the ceramic needles. Moreover, the needles proved to be capable of piercing the stratum corneum of the porcine skin. Promising results were obtained with this study opening the opportunity to deeply explore the fabrication of MN by self-setting ceramics and their capability to deliver drugs throughout the skin.

1.3 - Calcium phosphates

Calcium phosphates (CaPs) are the most important inorganic constituents of biological hard tissues. In the form of carbonated hydroxyapatite, they are present in bone, teeth and tendons to give to these organs stability, hardness and function. Calcium phosphate crystals are also found in nature as mineral deposits in considerable amounts, growing over the years, sometimes in extreme conditions of pressure and temperature. In contrast, biologically formed calcium phosphates are often nanocrystals precipitated under mild conditions (ambient pressure, near room temperature) [77].

Apart from calcium pyrophosphate ($Ca_2P_2O_7$), most calcium phosphates, previously used *in vivo* as bone substitutes in various forms, were calcium orthophosphates (presence of the orthophosphate group PO_4^{3-}), commonly named calcium phosphates (Table 1).

Table 1 -Some calcium phosphate compounds, their Ca/P ratios and symbols [78].

Name	Formula	Ca/P	Symbol
Monocalcium phosphate monohydrate	$Ca(H_2PO_4)_2.H_2O$	0.50	MCPM
Dicalcium phosphate dihydrate	$CaHPO_4.2H_2O$	1.00	DCPD
Calcium deficient hydroxyapatite	$Ca_{10-x}(HPO_4)_x(PO_4)_{6-x}(OH)_{2-x}$	1.50-1.67	CDHA
Amorphous calcium phosphate	$Ca_3(PO_4)_2.nH_2O$		
α-Tricalcium phosphate	α-$Ca_3(PO_4)_2$	1.50	α-TCP
β-Tricalcium phosphate	β- $Ca_3(PO_4)_2$	1.50	β-TCP
Sintered hydroxyapatite	$Ca_5(PO_4)_3OH$	1.67	HA

Among the numerous calcium phosphate compounds, only the precursor compounds used in this work will be referred and highlighted.

MCPM is the most soluble and acid for almost all pH levels [78]. It can be obtained by chemical precipitation from highly acidic solutions at room temperature with a crystalline structure similar to thin blades [79]. At temperatures above 100 ºC, a water molecule is released and MCPM is transformed into MCPA (anhydrous monocalcium phosphate). Due to his acidity and solubility, MCPM is not biocompatible, although it can be used in combination with other basic calcium phosphates for the production of several calcium orthophosphate cements [78], [79].

Many calcium phosphate cements (CPC) have been proposed as bone substitutes, some based on the use of tricalcium phosphate ($Ca_3(PO_4)_2$, TCP) [80]. TCP has three polymorphs [81] depending on the temperature, The low temperature β-TCP phase (rhombohedral structure - space group R3cH and theoretical density, 3.07 $g.cm^{-3}$) is obtained by thermal decomposition at temperature above 700-800ºC [82] and is stable up to 1125ºC. Above this temperature, α-TCP is transformed with volumetric expansion into the monoclinic α-TCP phase (theoretical density, 2.86 g cm^{-3}), which has a complex crystal structure with the space group $P2_1/a$. α-TCP is stable between 1125°C and around the temperature range of 1430ºC [83] - 1475 °C (as shown in phase diagram of Figure 4), and it can be maintained at room temperature as a metastable phase.

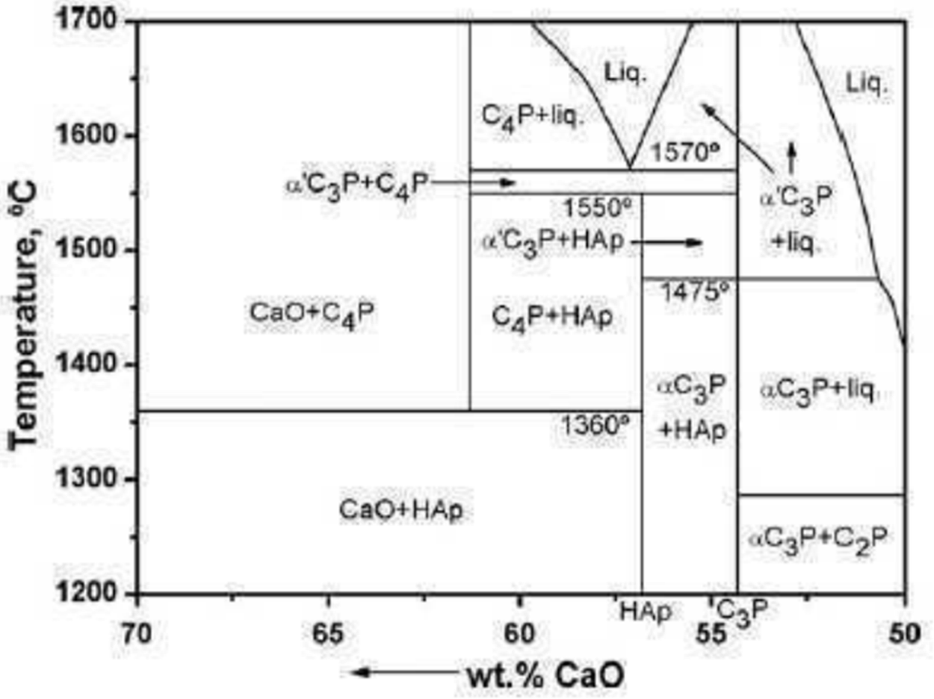

Figure 4- Phase equilibrium diagram for the $CaO-P_2O_5-H_2O$ system (C=CaO; $P=P_2O_5$; Ap=apatite) according to Riboud-[150].

The α′-TCP is stable above 1430°C – 1475ºC until the melting point of 1765ºC and is unable to survive quenching to room temperature [9-11].

Phase transformation through thermal treatment is the most direct way of obtaining pure α-TCP from β-TCP [84], but is also a challenging one. Small quantities of β-TCP [78-82] and/or HA [85-87] in the final product have been reported, resulting in non-pure, and therefore, unwanted biphasic composition. The presence of β-TCP as second phase is attributed to a partial reversion during cooling of the already formed α-TCP phase [88]. As the polymorphic β→α-phase transformation is considered to be reconstructive [85-87], the reverse α→β-TCP transformation would require surpassing a considerable activation energy barrier to proceed [89]. Considering this, reverting α→β-TCP should only be possible under a very slow cooling rate or a long dwell at a temperature below the transformation temperature. Rapid cooling techniques such as quenching [88-89] or a moderate to high cooling rate [89] (5ºC/min [92] and 10 ºC/min [93]) are suggested as a solution to maintain the desired α-TCP purity.

Besides the influence of temperature in phase conversion, some studies have showed that slight variations in Ca/P ratio (Ca/P=1.50) of TCP also affect α-TCP purity, as shown in the phase diagram presented above (Figure 4). These variations lead to the formation of small amounts of HA (positive variation, Ca/P > 1.50) or CPP (calcium pyrophosphate, negative variation, Ca/P < 1.50), as seen in Figure 5. Minor amounts of CPP are known to strongly affect the α↔β-TCP phase transition, as shown by Bohner et al. [93], Welch and Gutt [94], and more recently by Torres et al. [95]. Starting from a β-TCP powder with a trace of CPP to obtain pure α-TCP powder is compromised, with strong possibility to have in the final product β-TCP as secondary phase, which amount varies according to the cooling rate imposed on the calcination cycle.

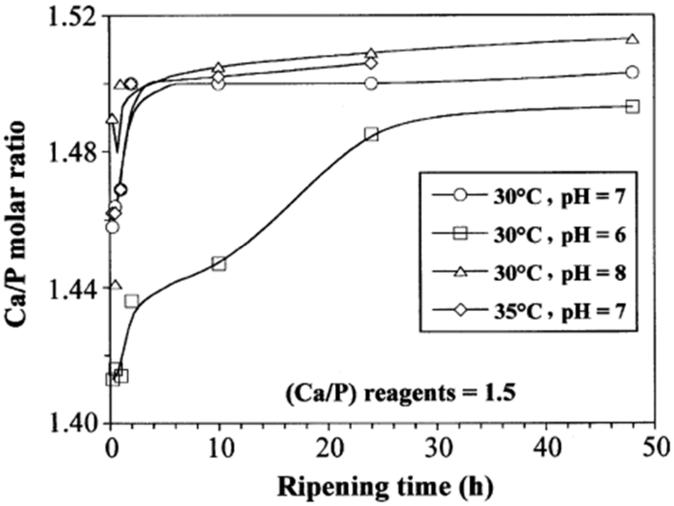

Figure 5- Ca/P molar ratio of precipitates vs. ripening time for different synthesis conditions of aqueous precipitation method according to Destainville et al. [96].

As shown by the work of Destainville et al. [96], a tight control over experimental conditions during the synthesis process, such as pH and temperature, greatly influence the resulting product. Figure 5 shows the Ca/P molar ratio versus the ripening time of powder synthesized at different temperature and pH values. For a temperature of 30ºC and pH 8, a Ca/P

> 1.50 is obtained in the first 4 hours, insuring that no CPP is formed and the α→β-TCP regression does not occur after thermal treatment.

β-TCP and α-TCP have been extensively used in medical applications due to the biodegradable and biocompatible properties [78, 97]. Considering its biological interactions, α-TCP is non-toxic, osteoconductive and bioactive. Although its biodegradability is higher than β-TCP and HA, it is less stable and as so, more reactive [98]. Calcium phosphates can also be categorized by one of their most important characteristics: solubility in aqueous medium. As so, depending on its chemical composition and porosity, CaPs can be organized by its degradability (ordered from more to less degradable) [78]:

MCPM > α-TCP > DCPD > DCP > β-TCP > HA

Properties like tension, compression force and stress resistance are also parameters highly dependent on the chemical composition and the porosity of the material that influences also its applications [99].

1.3.1 - Calcium phosphate cements

CPC's were first discovered by Brown and Chow in the 1980's [100]. Despite a large number of formulations, CPC are divided into two different end-products: apatite (CDHA) and brushite (DCPD) [78]. These synthetic biomaterials are formed from a mixture of a solid component and an aqueous solution, both reacting at room temperature to obtain a paste that contains one or more types of calcium phosphates [101], as summarized in the diagram presented in Figure 6 [102].

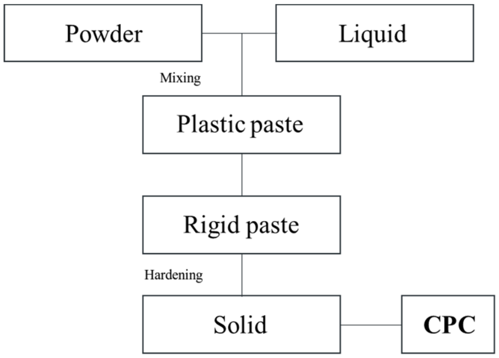

Figure 6- Preparation of a CPC. Adapted from: (Driessens, 1997) [102].

After mixing powder with liquid, a plastic paste is obtained, increasing viscosity as setting time increases, losing its malleability and ability to deform. During setting reaction, the calcium phosphates dissolve and precipitate into a less soluble CaP phase(s). The precipitated CaP crystals grow and become entangled, providing rigidity to the cement [78]. The chemical reaction occurring during the setting times of the CPCs is highly dependent on its chemical composition, and can be divided into two main types of reactions [103]:

(A) Acid-base reaction, as for example when the neutral β-TCP reacts with the acidic MCPM forming DCPC, as shown below (equation 1):

$$\boldsymbol{\beta\text{-}Ca_3(PO_4)_2\ (s) + Ca(H_2PO_4).2H_2O\ (s) + 7H_2O\ (l) - 4\ CaHPO_4.2H_2O\ (s)} \quad (1)$$

(B) Hydrolysis, when for example α-TCP is mixed with an aqueous solution, forming CDHA, or calcium deficient hydroxyapatite (equation 2):

$$\boldsymbol{3\ \alpha\text{-}Ca_3(PO_4)_2\ (s) + H_2O\ (l) - Ca_9(HPO_4)(PO_4)_5(OH)\ (s)} \qquad (2)$$

1.3.2 - Apatite CPCs

Since the discovery of CPCs [100], numerous formulations have been proposed. Most apatite CPC formulations have CDHA as the end-product of the reaction, having all of them a long intrinsic setting time [78]. The mechanical properties of the apatite CPC highly depend on its composition and can widely vary. The main factor is the ratio between the amount of setting liquid (L) and cement powder (P) that varies directly with the CPCs porosity (low L/P ratio results in low porosity), resulting in lower mechanical properties as the porosity increase. Considering the excellent biocompatibility of apatite CPCs, applications for drug delivery can be considered, as the CPC will not cause inflammatory response when in contact with skin [86].

1.3.3 - Brushite CPC

DCPD is the product of the setting reaction of so-called brushite cements. These types of cements where introduced by Mirtchi and Lemaitre in 1987 [35, 36], where the DCPD is a result of the β-TCP + MCPM reaction, as shown previously in equation (1). Several formulations to obtain brushite cements have been proposed, such as β-TCP + H_3PO_4 [97], [105] and β-TCP + MCPM + CaO [106]. According to Bohner et at. [105], the first formulation has some advantages over the second one: (i) rapid and easy preparation, (ii) better control over the chemical composition and reactivity, and (iii) better physical and chemical properties such as enhanced setting times and better tension resistance [105].

All brushite CPC are obtained via acid-base reaction, meaning that the paste is acidic during the setting reaction, since brushite only precipitates around $pH < 6$ [37, 39].

Brushite CPCs are biocompatible, bioabsorbable and rapidly degraded (in vivo conditions), due to their solubility [107] although the porosity has its influence. The high growth rate of the brushite crystals results in a low setting time, making it a material not suitable for certain clinical applications [108]. To somewhat compensate this flaw, additives such as citric acid [109] and glycolic acid [110], that inhibit the growth of DCPD crystal have been used to increase the setting time of the brushite CPCs. According to Román et al. [111] the hardening reaction (the complete formation of the crystals) of brushite has the duration of around 24 hours, for a Ca/P of 1.50 and using citric acid as liquid phase, although having a high initial reactivity. This is probably due to the fact that, at the end of the setting reaction, the pH level of the mixture increases, which causes a decrease in the solubility of the reagents [97].

1.3.4 - Apatite CPCs vs Brushite CPCs

Although both apatite and brushite cements are commercially available due to their usefulness for the reconstruction of bone defects, their behaviors in the bone defect are quite different especially in respect to resorption. Brushite cement resorbed much faster when compared to apatite one. This difference is caused by the compositional difference in the final products. As the name represents, final product of apatite cement is apatite, whereas final product of brushite cement is brushite being apatite the most thermodynamically stable phase at physiological conditions. Since the human body-fluid is supersaturated in ions of apatite phase, no physicochemical dissolution occurs in the case of the apatite cement (at physiological conditions) [112].

Brushite is the most stable phase at pH values in the range of 2.0–4.2 being formed based on dissolution-precipitation reaction and entanglement of the brushite crystals during setting reaction. However, brushite is a metastable phase at physiological pH and dissolves upon exposure to the body fluid [112].

Nonetheless, brushite cement dissolves much faster than apatite cement. As an example, Apelt et al.[113] reported that brushite cement was used for the reconstruction of bone defects in sheep, and it almost completely resorbed after 6 months, whereas apatite cement did not show any notable change for the same time period [45, 46].

1.3.5 - Properties of the CPCs

CPCs have wide range of properties that are tightly linked to several factors that can be tailored according to the application target, as shown in Table 2. The final properties of the CPCs depending highly on the composition of its solid phase, ratio of the components in the mixture, additives and particle size distribution of the powder.

Table 2- Parameters that affect the properties of the CPCs. From: (Ginebra, 2008)[107].

Powder phase	Chemical composition Relative proportion of its constituents Additives (accelerators, retardants) Particle size distribution
Liquid phase	Additives (accelerators, retardants, cohesion parameters) pH
Mixing parameters	Powder/Liquid ratio Mixture process (time, rotation)
Environmental factors	Temperature Humidity pH

Particle characteristics

The particle characteristics of powder phase heavily influence initial and final properties of CPC. Particle size and size distribution, shape and specific surface area are the four major influences of powder phase on the behavior of the CPCs. Particle size is directly related to the setting time and consequently to the mechanical properties of the CPC. For a given liquid to powder ratio setting time decreases as particle size decreases, since smaller particles dissolve faster and the precipitation process of the new phase begins earlier [93].

Liquid phase

The liquid phase composition in a powder-liquid mixture is also an important factor that influences final CPCs properties. The liquid is a vehicle for the dissolution of the reagents and for the precipitation of the final products of the reaction. This aqueous phase can be just composed of distilled water or can contain many organic or inorganic additives that can be used to tailor CPCs properties. These additives can influence the setting time, rheological, cohesive properties and porosity of the paste/cement, for example:

- Sodium hydrogenophosphate (Na_2HPO_4) [114]: accelerates the hardening process, lowering the setting times in apatitic cements;
- Citric acid ($C_6H_8O_7$)[109]: (1) slows the reaction time, increasing the setting time in brushitic cements; and (2) accelerates the hardening process in apatitic cements, decreasing the setting time.

Liquid-to-powder ratio

The liquid-to-powder ratio (L/P) is a very important parameter than can determine several properties of the cement [115], such as setting time [116,117], rheological behavior[115] and mechanical strength [98, 117]. Higher L/P ratios lead to a decrease in mechanical strength and higher initial (IST) and final (FST) setting times, which can be explained by the increase in porosity caused by the higher amounts of liquid phase [98,117].

Setting time

Setting time is defined as a specified time required for a paste/cement to change from liquid state to plastic state (initial setting time, IST) and plastic state to solid state (final setting time, FST), so that the surface becomes sufficiently rigid to withstand a defined amount of pressure [118]. It's a continuous process that can be described in three steps [119]:

1. Dissolution of the reagents;
2. Nucleation of the newly formed crystals;
3. Growth of the newly formed crystals.

There are two methods used to determine IST and FST of a cement, the Gillmore needle test [Standard Test Method for Time of Setting of Hydraulic-Cement Paste by Gillmore Needles, ASTM C266-15] and the Vicat needle test [Standard Test Methods for Time of Setting of Hydraulic Cement by Vicat Needle, ASTM C191-13]. Both of these tests follow the same methodology, analyzing the surface of the cement to assess if the needle produces an indent after contact [120]. The Gilmore needle test is more widely used, consisting of two different needles: (1) a thick and light needle to assess the IST and (2) a thin and heavy to determine the FST. The Vicat needle test, on the other hand, uses only one needle at a time to determine the IST or FST.

Evaluating the setting times of a cement is essential to determine its handling time of a cement past. For the molding process, up until the IST, the cement is malleable, so it can be deformed and molded to a desired shape. When the compound is in the desired shape and the hardening process is yet to be completed, it cannot be handled without the risk of producing fractures along the structure. The FST indicates when the hardening process is finish and the sample can be handled without damaging it. As in other properties, setting time can be influenced by different factors of the mixture (liquid and solid phases) as well as ambient conditions [107]:

i) Particle size;
ii) Crystallinity;
iii) Composition of the liquid phase;
iv) Temperature;
v) Liquid-to-powder ratio.

Mechanical Properties

The mechanical properties of CPCs are a key property that needs to be determined to assess if the composition of the cement is adequate for the intended use. Generally, CPCs have poor mechanical properties [121-124], limiting its clinical applications. As a method of enhancing these properties, some authors used polymers such as gelatin [125] and short-length polyhydroxyalkanoate (linear polyesters produced by bacterial fermentation of sugar or lipids) [126]. Several factors can influence the mechanical properties of CPCs, as shown in Table 3 [127].

Table 3- Properties of CPCs that can affect its mechanical behavior.

Property	Effect
Formulation [128]	Maximum shear resistance can vary for formulation to formulation.
Liquid-to-powder ratio [129]	A higher L/P ratio leads to a decrease in shear resistance.
Particle size [130]	As the particle size decreases, the shear resistance increases.
Incubation temperature [131]	High temperatures can lead to the dehydration of the samples, weakening its structure.

In a recent study published by Ingrid Ajaxon et al.[132] the compressive strength and elastic properties of brushitic and apatitic CPCs were measured and compared. The brushitic CPCs were found to be stronger than the apatitic CPCs, in good agreement with other results presented in literature [80,91,103,133,134].

Porosity

Water is a major intervenient in the setting reaction of CPCs, as shown in previous equations (1) and (2). As a result, not all the water is consumed during the hydration phase, resulting in a porous structure. The porosity of CPCs is directly related to the L/P ratio used varying between 30% and 50%. Particle size distribution of the starting powders and particles packing behavior can also modify the microstructure, as well as the pores size and size distribution [135]. Techniques such as mercury intrusion porosimetry (MIP) [136], gas adsorption and thermoporometry (TPM) [137] and have been used to determine the porosity of CPCs [138].

Chapter 2:
Materials and Methods

2. Materials and Methods

In order to better understand how this thesis was conducted, the experimental work will be divided into five stages of production. Each stage includes the characterization techniques that are required to either move forward to the next stage or to better understand its results. Stages are divided as follows:

Table 4- Description of the different stages of the developed work

	Description	*Characterization techniques*
Stage 1	Synthesis of CaP based powders	pH and temperature monitoring
Stage 2	Calcination and milling of powders	Particle size and size distribution Crystalline phases
Stage 3	Preparation and moulding cement pastes with and without drug	Setting time Mechanical properties Porosity and density Crystalline phases Microstructural analysis (SEM)
Stage 4	Antibiotic distribution and release studies	Raman Confocal UV
Stage 5	Microneedles fabrication	SEM Mechanical properties

2.1 - Stage 1: Synthesis of CaP based powders

To obtain brushitic and apatitic cement pastes, TCP (β-TCP powder) and BTCP (biphasic powder, mixture of β-TCP and α-TCP) were used as starting materials. These CaP based powders where synthesized via wet chemical precipitation method according to previous works [127].

The synthesis process starts with the preparation of aqueous solutions (deionized water) of diamonium hydrogenophophate, ($[(NH_4)_2HPO_4.4H_2O]$, Panreac, Spain) and calcium nitrate tetrahydrate, ($[Ca(NO_3)_2.4H_2O]$, Panreac, Spain) as phosphorous and calcium precursors, respectively. In order to obtain a Ca/P ratio of 1.51, a 0.6M of P solution was used and the Ca concentration was adjusted accordingly. Although the theoretical value of Ca/P ratio to obtain pure β-TCP is 1.50, a Ca/P ratio of 1.51 was used to ensure that no β-CPP (calcium pyrophosphate) was formed. The solutions were mixed inside a reactor at 30ºC and stirred at 700 rpm for 4 hours. The pH levels were monitored in real time, as described below. pH was adjusted to 7-8 using an ammonia solution (25% NH_3, Sigma-Aldrich, Germany) with a final added volume ranging from 100 mL to 150 mL. After 4 hours, the precipitate was vacuum filtered and dried at 100ºC for 72h. The full process is schematically presented in Figure 7. A total of nine synthesis were performed, hereafter denominated as S-I, S-II, S-III, S-IV, S-V, S-VI, S-VII, S-VIII, S-IX, in order to have enough powder for the desired assays, resulting in 200-250 g of powder per synthesis.

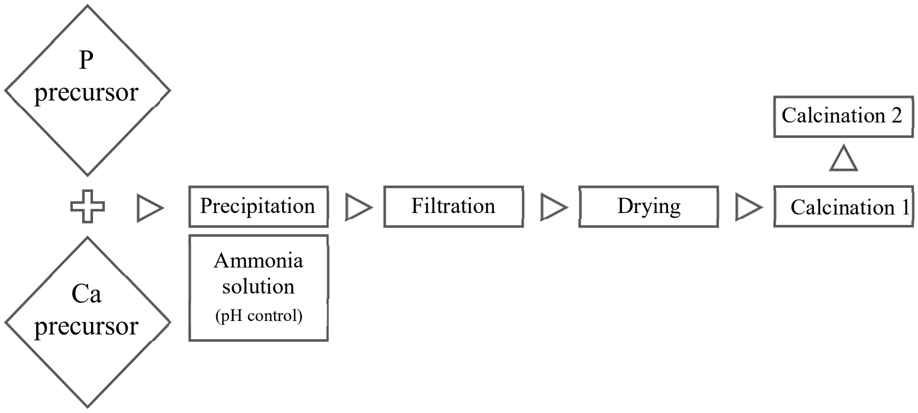

Figure 7- Schematic representation of the method used to obtain the CaP based powders.

2.1.1 - pH and temperature monitoring

As described in previous works [127], experimental conditions such as Ca/P ratio, synthesis time, pH and temperature, are essential to obtain the desired powder composition. For the standard synthesis conditions available in the lab, the pH is not continually measured and the temperature evaluation is relied on the oil bath recirculation to maintain the targeted 30ºC within the reactor. Since small fluctuations in pH could influence the final products, a data logger (DrDAQ, PICO) coupled with a pH sensor (DD011) connected to a laptop running a logging software (PICOlog) were used in order to monitor the pH in real time, obtaining values every second (Figure 8). This allowed a more precise control over pH conditions and an overall optimization of the reaction, raising the number of control points from ≅30 to 14400. Regarding temperature, it was monitored by a digital thermometer equipped with a metal rod every 5 minutes. The obtained data (.txt file) was processed using MatLab to automate the process. In order to better represent the data, every 10 minutes a total of 10 control points ([-5s, +5s]) were chosen, its average value calculated and then plotted.

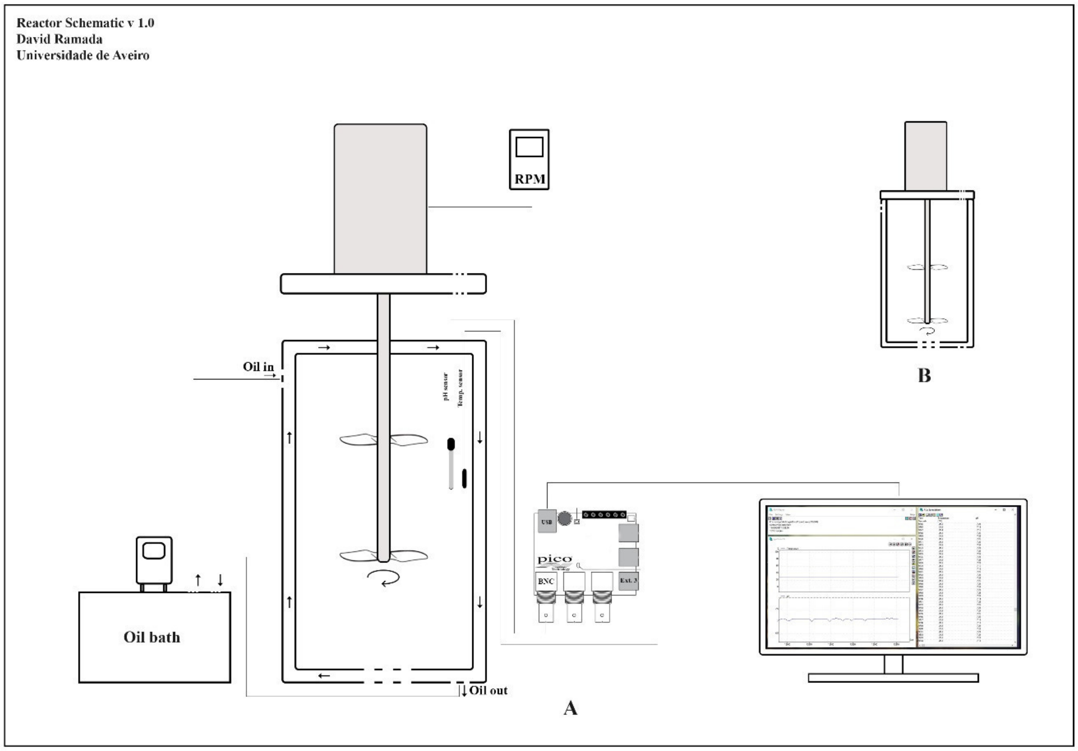

Figure 8- Reactor schematic. The oil bath maintains the desired temperature during the reaction (left). PICO data logger was used to monitor temperature and pH in real time.

2.2 - Stage 2: Calcination and milling of CaP based powders

The dry precipitates were deagglomerated and then calcined. To obtain TCP, the CaP based milled powder was calcined in a Termolab furnace at 1000ºC maximum temperature with 2h holding time with a heating rate of 5ºC/min, followed by natural cooling to ambient temperature. To obtain BTCP, previously β-TCP powder was submitted to 1250ºC maximum temperature with the following schedule [127]: 10ºC/min until 1000ºC, followed 5ºC/min to 1250ºC, with 10h holding time at this temperature with subsequent cooling to 30ºC at 20ºC/min rate. Figure 9 summarizes the calcination schedules used to obtain both powders. After cooling, both powders were milled and analyzed in terms of particle size distribution and crystalline phases.

2.2.1 - Particle size distribution (PSD) analysis

Particle size distribution was determined using a Coulter LS 230 (Fraunhofer optical model, United Kingdom), allowing a measurement of particles in the range of 0.4 µm-2000

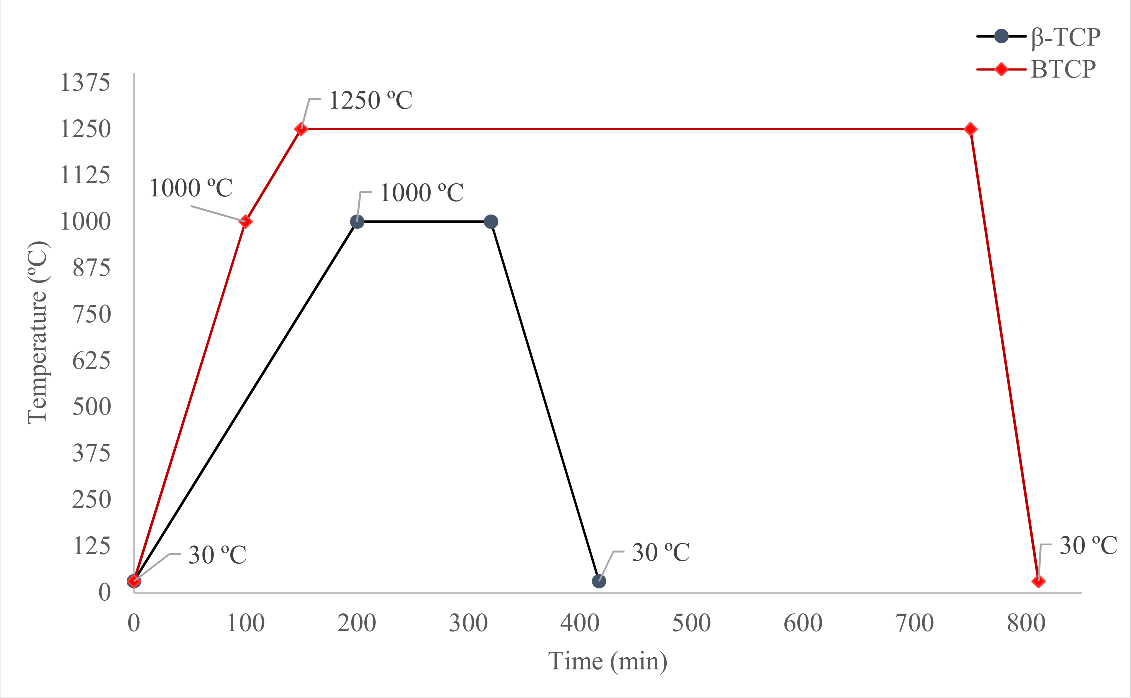

Figure 9 - Calcination schedules used to obtain TCP (β-TCP) and BTCP (β-TCP+α-TCP) powders.

μm. For that, the powders were dispersed in an aqueous medium with a few drops of deflocculant (Targon 1128, BK Giulini Chemie, Germany) for deagglomeration and ultra-sonicated for 5 minutes at ambient temperature.

2.2.2 - Crystalline phase

The crystalline phases of both CaP based powders (TCP and BTCP) were determined via X-ray diffraction (XRD) using a high resolution diffractometer (Bunker D8 Advance DaVinci) with Cu-Kα radiation at a wavelength of λ=1.5406 Å, scan interval (2θ) of 5º to 70º and a step width of 0.0130º 2θ.s^{-1}. The identification of the crystalline phases was evaluated comparing the obtained diffractogram to the standard diffractograms listed below in Table 5:

Table 5 - Standard JCDD cards used for the crystalline phases identification.

Name	Symbol	PDF number
Calcium deficient hydroxyapatite	CDHA	01-071-6794
Dicalcium phosphate	DCP	04-009-3755
Dicalcium phosphate dihydrate	DCPD	04-013-3344
Sintered hydroxyapatite	HA	04-015-7245
α-Tricalcium phosphate	α-TPC	04-010-4348
β-Tricalcium phosphate	β-TCP	04-006-9376
β-Tricalcium pyrophosphate	β-CPP	04-009-3876

2.3 - Stage 3: Preparation and casting cement pastes with and without antibiotic

As described in chapter 1.3, to obtain a cement paste, a solid phase is mixed with a liquid phase. In the present work, two cement paste compositions have been prepared to obtain brushitic and apatitic cements. The system β-TCP + MCPM (Monocalcium phosphate monohydrate, [$Ca(H_2PO_4)_2.H_2O$], Sigma-Aldrich, Germany) mixed with citric acid aqueous solutions (15%, [$C_6H_8O_7$], Sigma-Aldrich, Germany) was used for brushitic cements preparation, while BTCP mixed with 3wt% of anhydrous sodium hydrogen phosphate [Na_2HPO_4] (Merck, Germany) or citric acid (10-15%) were used to obtain apatitic or brushitic cements, respectively [120]. The pastes were prepared by adding the powders with different amounts of liquid phase according to the desired liquid to powder ratio: 0.28, 0.30, 0.34, 0.38 and 0.40 mL.g^{-1}. For cements loaded with antibiotic, 2.5 wt.% of levofloxacin was added to the paste. All pastes were then casted in different mold shapes according to characterization requirements (pellets, cylinders or microneedles). The molded samples were then placed in an oven with controlled temperature and humidity (37ºC, with a set humidity of 80%) for the time required for setting and subsequently de-molded and kept in the same condition for further 96 h. After this period, in order to study the probability of drug migration to the surface of the samples, two different drying processes were used: (1) cement samples were placed at 40ºC without controlled humidity until complete drying (oven drying, OD); (2) samples were immediately frozen at -80ºC for 48h and then lyophilized for 24h (freeze drying-Liof). Figure 10 resumes the full process.

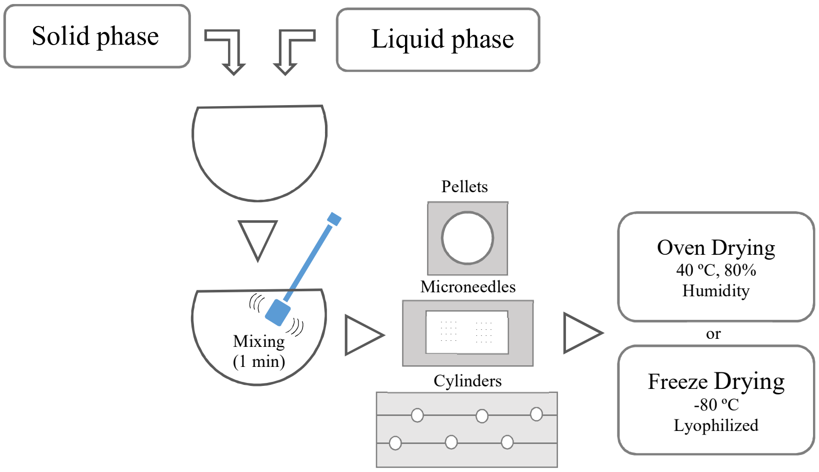

Figure 10- Schematic procedure of preparation, molding and drying of the cement samples. Each sample is prepared accordingly and then molded into the correct shape for the desired essay. After de-moulding, samples are either oven dried or lyophilized.

The CPC formulations studied are listed in Table 6 and 7, for cements prepared from TCP and BTCP powder, respectively, as well as the nomenclature used for each of them.

Table 6: CPC formulations prepared from TCP powders.

Nomenclature	L/P ratio ($mL.g^{-1}$)	Citric acid (wt.%)	Levofloxacin (wt.%)
Oven drying			
TCP-0.28-OD	0.28	15	-
TCP-0.30-OD	0.30	15	-
TCP-0.30-L-OD	0.30	15	2.5
TCP-0.34-OD	0.34	15	-
TCP-0.34-L-OD	0.34	15	2.5
Lyophilization			
TCP-0.28-Liof	0.28	15	-
TCP-0.30-Liof	0.30	15	-
TCP-0.30-L-Liof	0.30	15	2.5
TCP-0.34-Liof	0.34	15	-
TCP-0.34-L-Liof	0.34	15	2.5

Table 7 - CPC formulations prepared from BTCP powder.

Nomenclature	L/P ratio ($mL.g^{-1}$)	Liquid composition Citric acid (wt.%)	Liquid composition Na_2HPO_4 (wt.%)	Levofloxacin (wt.%)
Oven drying				
BTCP-0.28-HP3-OD	0.28	-	3.0	-
BTCP-0.30-HP3-OD	0.30	-	3.0	-
BTCP-0.34-HP3-OD	0.34	-	3.0	-
BTCP-0.38-HP3-OD	0.38	-	3.0	-
BTCP-0.40-HP3-OD	0.40	-	3.0	-
Lyophilization				
BTCP-0.34-AC10-L-Liof	0.34	10	-	2.5
BTCP-0.34-AC15-L-Liof	0.34	15	-	2.5

2.3.1 - Setting time (IST and FST)

Initial setting time (IST) and final setting time (FST) of the cement pastes were determined using a Gillmore needle apparatus, as stated in the norm ISO/DIS 18531:2015 (E). After mixture, the cement paste is poured into a silicone mold (3 cm in diameter, 1 cm thick) and placed in a closed box (with a relative humidity ≥70%). For IST purposes the lower weight needle was used while for FST was used the heavy needle. The measurements consist in pouring the needle onto the surface of the cement sample every 30s and observing if an indentation is formed. The process was repeated until no indentation was visible in the cement surface, being this times IST of FST.

2.3.2 - Mechanical properties

The cement pastes were casted into cylinders (as shown in Figure 10) (Φ 6 mm, height: 12 mm) for compressive strength measurements. For all cylinders, parallel base surfaces were assured (rectifying if not parallel) and its mechanical properties were tested using a Shimandzu Autograph (Japan), equipped with a 10 kN load cell (Figure 11). Each cylinder was placed between the pressure plates and compressed until failure at a strain rate of 1 $mm.min^{-1}$.

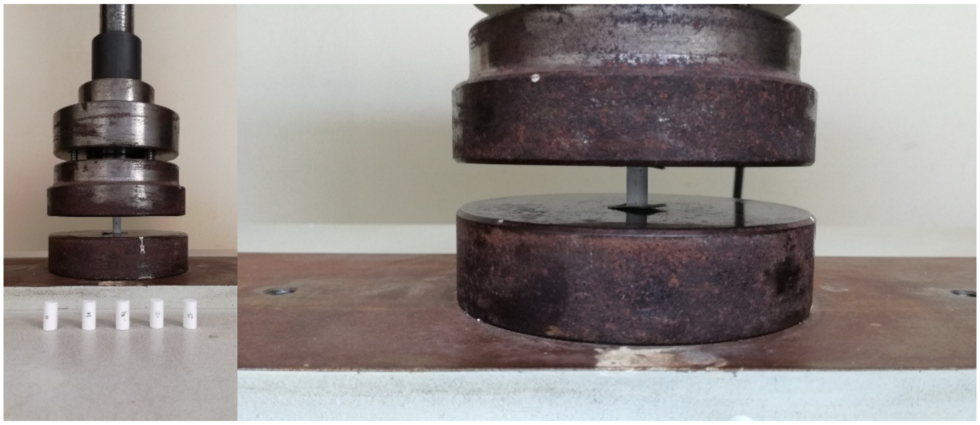

Figure 11- Cylindrical cement samples used for compressive strength test (left) and cement sample ready to be tested (right).

To access the force that can be applied to the microneedle tip without breakage, was used the apparatus presented in Figure 12 .

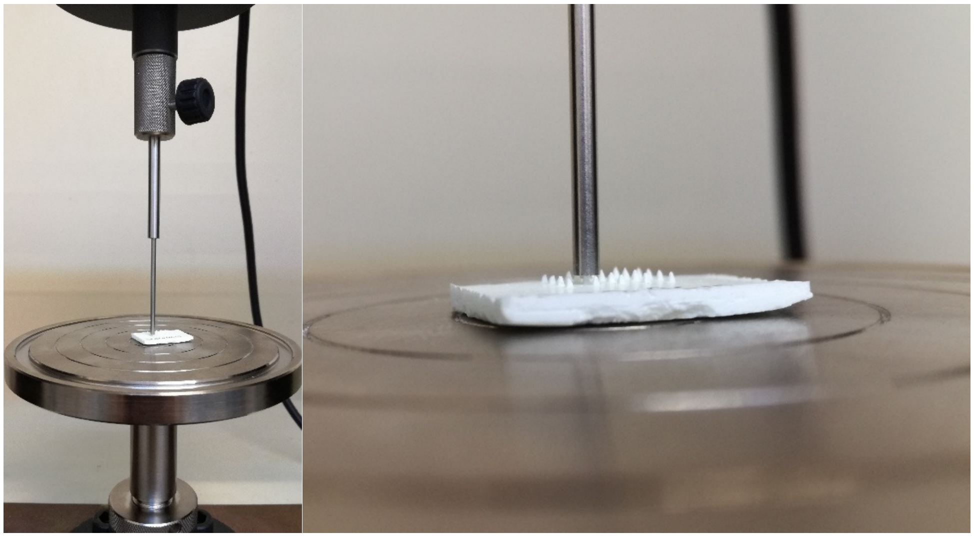

Figure 12 - Apparatus used to access the mechanical properties of the microneedle tips.

2.3.3 - Porosity and density

The total porosity (open and closed porosity) was determined from the real density and the apparent density, as shown in equation 3:

$$\text{Total porosity} = \frac{\text{Real density} - \text{Apparent density}}{\text{Real density}} \quad (3)$$

where,

- *Open porosity:* network of fine interconnected capillaries, connected to the surface of the material;
- *Closed porosity:* pores with no connection to the surface;
- *Apparent density:* ratio between the weight and the apparent volume of a sample. Dried cement samples (40ºC for 4 days) were weighted and their apparent volume determined according to the Archimedes principle by immersion in mercury, as presented in previous works [127]. The apparatus used for this measurement was presented in Figure 13.
- *Real density*: difference between the apparent volume of the sample and the total volume of pores (open and closed), which was determined by a Helium pycnometer (Multipycnometer Quantumchrome, US). For this test, dried and milled cement samples were used.

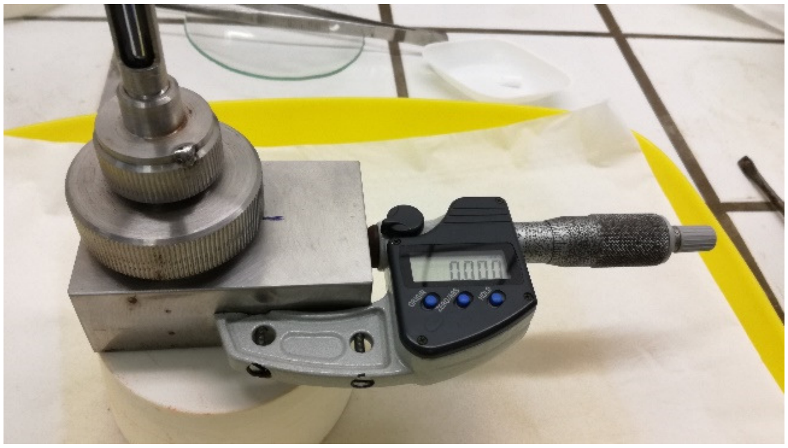

Figure 13- Apparatus used to determine apparent volume of cement samples according to Archimedes Principle.

2.3.4 – Microstructural analysis

Scanning Electron Microscopy (SEM, Hitachi S-4100, Japan), was used to determine the microstructural properties of the samples. The microscope is equipped with an electron emission system with a tungsten filament, and all the images were taken with an acceleration of 25 kV at different magnifications. Surface of the cement samples were observed.

2.4 - Stage 4: Antibiotic distribution and release studies

In this stage of the thesis, antibiotic distribution in cement samples and release studies were carried out. Samples loaded with 2.5% of levofloxacin (oven dried and lyophilized) were analyzed via Raman using a confocal Raman microscope (WITec alpha300 RAS+ (WITec, Ulm, Germany). An Nd:YAG laser operating at 532 nm were used as excitation source, with the power set 5mW (150 x 150 points per grid in a 50 x 50 µm area, 2s) to access the drug distribution on the samples. Drug release studies were carried out on the Faculty of Pharmacy, Universidade Nova, Lisbon.

2.4.1 - Preparation of the samples

During preparation of levofloxacin loaded cement pastes with biphasic powder (BTCP) using anhydrous sodium hydrogen phosphate as liquid phase composition, it was verified that resulting cement paste exhibited two phases (liquid and solid) instead of one (as per usual with the samples without levofloxacin). This phenomenon was attributed to the lower solubility of the levofloxacin in basic solutions when compared to acidic solutions. In order to verify this issue, the pH of the two used liquid phases (anhydrous hydrogen phosphate and citric acid) was measured and, as expected, the citric acid solution has a pH of 1.65, compared to the 8.58 pH value of the anhydrous sodium hydrogen phosphate solution. High pH values causes insolubility of levofloxacin and consequently, the hindrance of cement setting with subsequent phases separation. To overcome this problem, it was decided to use citric acid (10%) as liquid phase for BTCP levofloxacin loaded samples for release studies.

Accordingly, cement samples were prepared using the formulations described in Table 8. The resulting pastes were molded into cylinders (height: 12 mm; diameter: 6 mm), incubated for 24 h (37.5ºC, 80 % humidity), frozen for 2 days (-80ºC) and lyophilized. In order to assess the influence of the lyophilization on the drug release rate, samples from batch 2 (Table 8, TCP-0.30-L-OD and TCP-0.30-OD) were placed 4 days in a drying oven at 40ºC (Oven dried) instead of being frozen and lyophilized.

Table 8 - Batch formulations of the CPCs used.

Precursor Powders (P)	Liquid medium (L), Concentration (w/v %)	L/P (mL g^{-1})	Drying method	Levofloxacin (w %)	Cement Formulation Name	
β-TCP + MCPM	Citric acid, 15 %	0.30	Lyophilisation	2.5	Batch 1	TCP-0.30-L-Lyof
β-TCP + MCPM	Citric acid, 15 %	0.30	Lyophilisation	0.0		TCP-0.30-Lyof
β-TCP + MCPM	Citric acid, 15%	0.30	Oven dried	2.5	Batch 2	TCP-0.30-L-OD
β-TCP + MCPM	Citric acid, 15%	0.30	Oven dried	0.0		TCP-0.30-OD
β-TCP + MCPM	Citric acid, 15 %	0.34	Lyophilisation	2.5	Batch 3	TCP-0.34-L-Lyof
β-TCP + MCPM	Citric acid, 15 %	0.34	Lyophilisation	0.0		TCP-0.34-Lyof
BTCP	Citric acid, 10 %	0.34	Lyophilisation	2.5	Batch 4	BTCP-0.34-L-Lyof
BTCP	Citric acid, 10 %	0.34	Lyophilisation	0.0		BTCP-0.34-Lyof

2.4.2 - In vitro drug release assay

Levofloxacin loaded cylindrical samples were tested in order to determine the drug release profile and kinetics. For this study, 3 levofloxacin loaded cylinders and one blank (without loaded drug) from each batch formulation were used, amounting to a total of 16 samples. Samples were accurately weighted, placed on a 50 mL Falcon tube and immersed in 25 mL of a biomimetic medium (phosphate buffer saline, PBS, Sigma-Aldrich) at pH 7.4. The tubes were then placed on a 37ºC water bath (Memmert, Germany) and shaken horizontally (130 rpm) during the assay (72 h) (Figure 14A).

At pre-determined times of 10 min, 0.5h, 1h, 2h, 4h, 6h, 8h, 24h, 48h and 72h, 5 mL of each medium was collected (and replaced with the same volume of fresh medium) and analysed via UV-spectrometry, at 288 nm in a multiplate reader (FLUOstar Omega, BMG Labtech) in

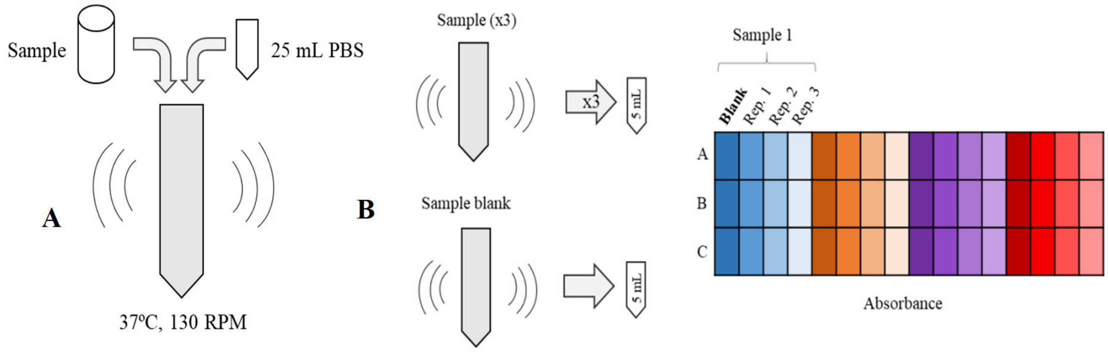

Figure 14- Schematic representation of drug release studies procedure. Each sample is immersed in a PBS medium and placed on a 37ºC water bath (A). After a certain time point is reached, 200 µL aliquots from each sample (and blank) are transferred in triplicate (rep. 1 to 3) to a 96-well microplate and analyzed via UV-spectrometry at 288 nm (B).

triplicate, as shown in Figure 14B. The absorption of the medium collected from the correspondent blank samples at the same time points were used as controls.

Calibration curves were prepared in PBS medium with 7 standards (i.e. 75, 65, 50, 40, 25, 15 and 5 µg mL^{-1} of levofloxacin). The absorbance of PBS was also measured to be used as blank. The calibration curves were repeated for each time point and 3 replicates were considered for each standard. The standards were prepared from a levofloxacin stock solution (with a concentration of 500 µg mL^{-1}, obtained by the dissolution of 125 mg into 25 mL PBS,) maintained at 37ºC during the assay.

The main assessments made during the release study are as follows:

i. Levofloxacin release profile (over a 72h period);
ii. Release kinetics.

Following the results of the antibiotic release essay, the best formulations were then used to fabricate the microneedles.

2.5 – Stage 5: Microneedle fabrication

The preparation of the cement pastes for the microneedles casting was conducted as described in section 2.3. The prepared pastes were then poured into a mold as seen in Figure 15. Several casting processes were used to obtain the best filling results (filling full length of the needle):

i. *Manual casting:* the pastes were poured into the mold and pressed downwards with a spatula;
ii. *Vacuum casting:* the pastes were poured into the mold and placed in a vacuum chamber;
iii. *Ultrasound casting:* after pouring the pastes into the mold, the mold was then placed into a Petri dish and sonicated.

The manual filling was the technique that produced the best results and was the one used throughout this thesis. Mechanical properties and SEM imaging were used to characterize the samples, according to the procedure described in section 2.3.2 and 2.3.4, respectively.

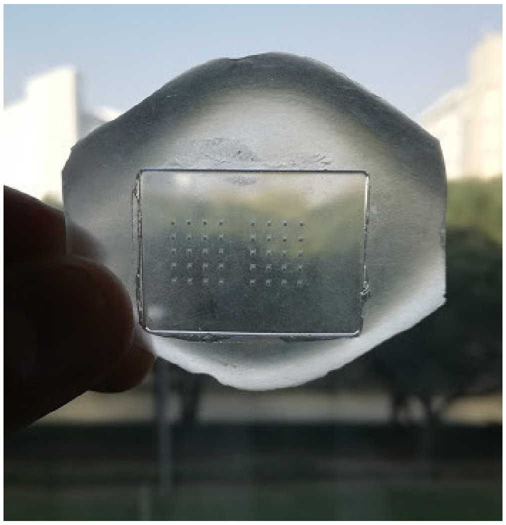

Figure 15- Silicon molds used to produce the microneedles.

Chapter 3:
Results and Discussion

3. Results and Discussion

3.1 - Characterization of the starting powders

As stated in Chapter 2, CaP based powders where synthesized via wet chemical precipitation method, where a close monitoring of the pH and temperature was made during the full complete synthesis time (180 min). These two parameters are of paramount importance since they influence the phases formed. pH evaluation with time for all nine synthesis is plotted in Figure 16, while average temperature measurements for each synthesis are presented in Figure 17.

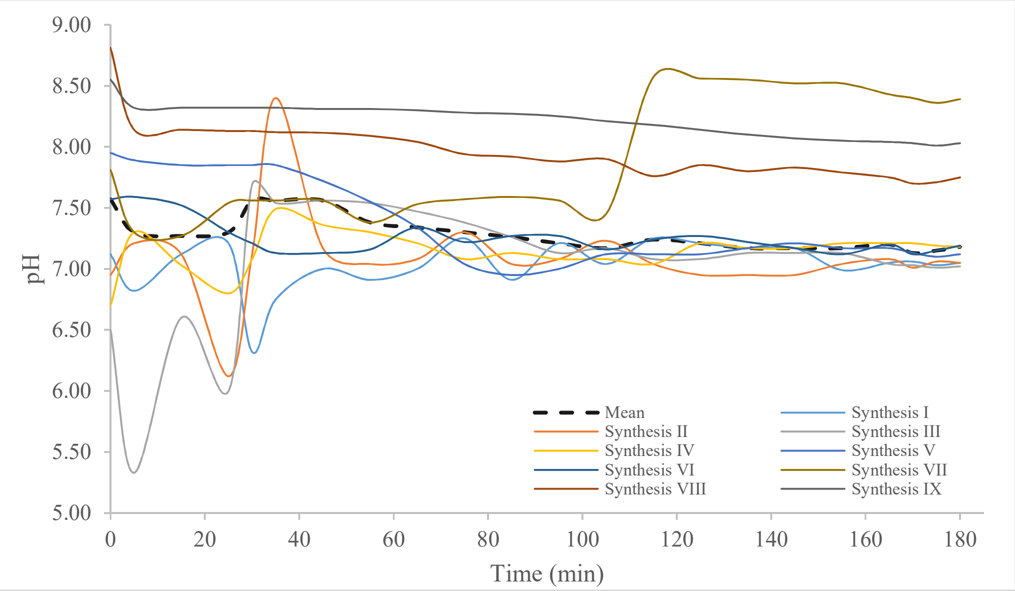

Figure 17 - pH values throughout the duration of the reaction for synthesis I to IX.

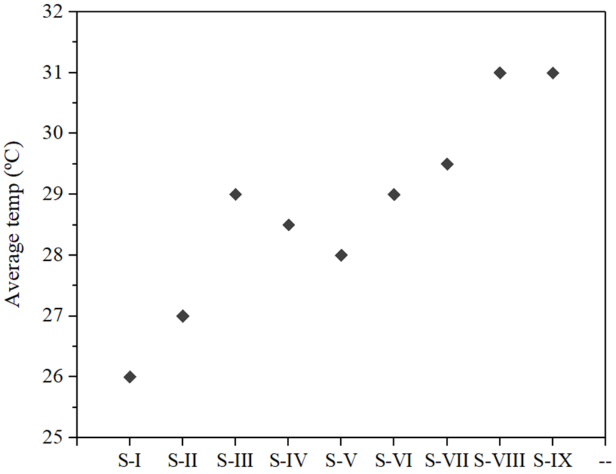

Figure 16 - Average temperature values for synthesis I to IX.

As seen in Figure 17, the temperature could not be maintained at a steady 30ºC being observed slight variations in the several syntheses evaluated (S I-IX). Concerning pH, higher variations are observed in the first hour attaining more stable values from this time to the end of the synthesis. Oppositely, synthesis S-VIII and S-IX presents the highest pH values almost stable (pH 8 - 8.5) throughout full synthesis time, resulting from the higher amount of ammonia added in the beginning of the synthesis.

The dried powders resultant from the previous synthesis were then calcined (first calcination at 1000ºC/2h holding time). X-ray diffraction was used to identify crystalline phases of the powders in all the synthesis evaluated (S - I to IX). Figure 18 presents the results obtained.

For the experimental conditions used (Ca/P = 1.51, pH 7-8 and 30 ºC) powders from S-II, III, VII, VIII and IX presented β-TCP as its main phase with different amounts of HA as secondary phase, except for powders resultant from S-I, IV, V and VI which seemed to be pure β-TCP. The existence of HA in some powders could be explained by the fluctuations in pH and temperature observed during their synthesis (Figure 16 and 17, respectively), essentially in the first hour of the synthesis. None of the synthesized powders presented a detectable β-CPP phase being a good indication for going further with β-TCP to α-TCP transformation, since is stablished from a previous work that a β-CPP phase produces an undesired effect in the β→ α-TCP transformation [95, 127]. However, detecting low quantities of β-CPP phase by X-ray diffraction is not an easy task, as its most intense ($2\theta = 29.6$ º) and second most intense ($2\theta = 27.6$ º) peaks overlap the β-TCP peaks. Only the third most intense peak ($2\theta = 28.9$º), not being overlapped by any other peak, is used to identify this phase. Oppositely, traces of HA phase are easier to identify, with its most intense peak ($2\theta =31,8$ º) not overlapped by any of the β-TCP peaks.

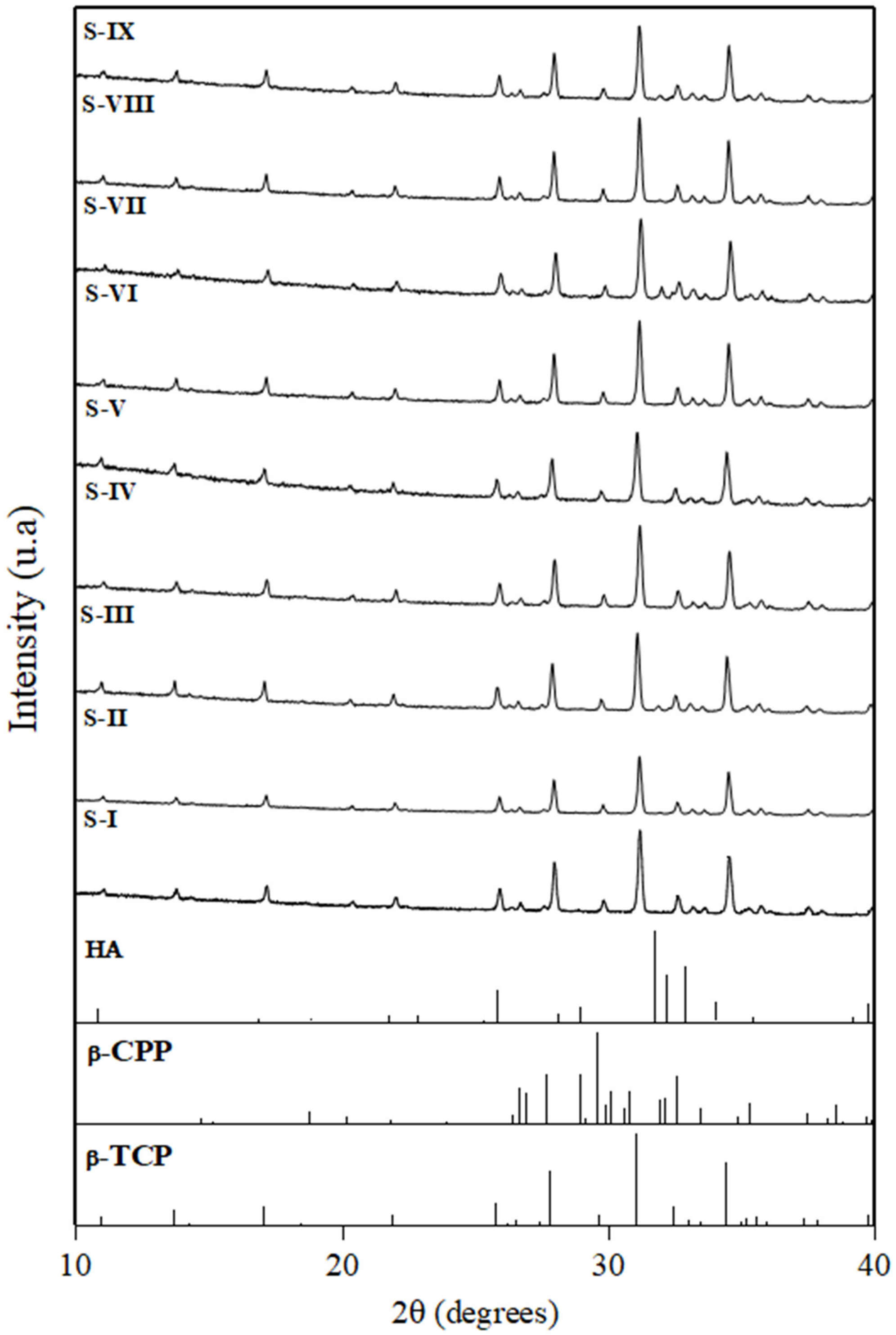

Figure 18 - Diffractogram of the calcined powders resultant from synthesis I-IX. The standard JCDD PDF (codes in Table 5, section 2.2.2) of HA, β−TCP and CPP are also presented for comparison.

According to these results, powders from S-I, IV, V and VI were selected to proceed with further studies with β-TCP powder. Powders from S- II, III, VII, VIII and IX were mixed and then submitted to the second calcination in order to obtain α-TCP. Unfortunately, powders II and III were mislabeled for V and VI, by mistake. So, in reality, the following mixtures were obtained: S-I, II, III and IV for following with TCP studies and S-V, VI, VII, VIII and IX for going further for β to α-TCP transformation (second calcination at 1250ºC/10h holding time). Figure 19 presents the XRD results of the resultant powder after the second calcination.

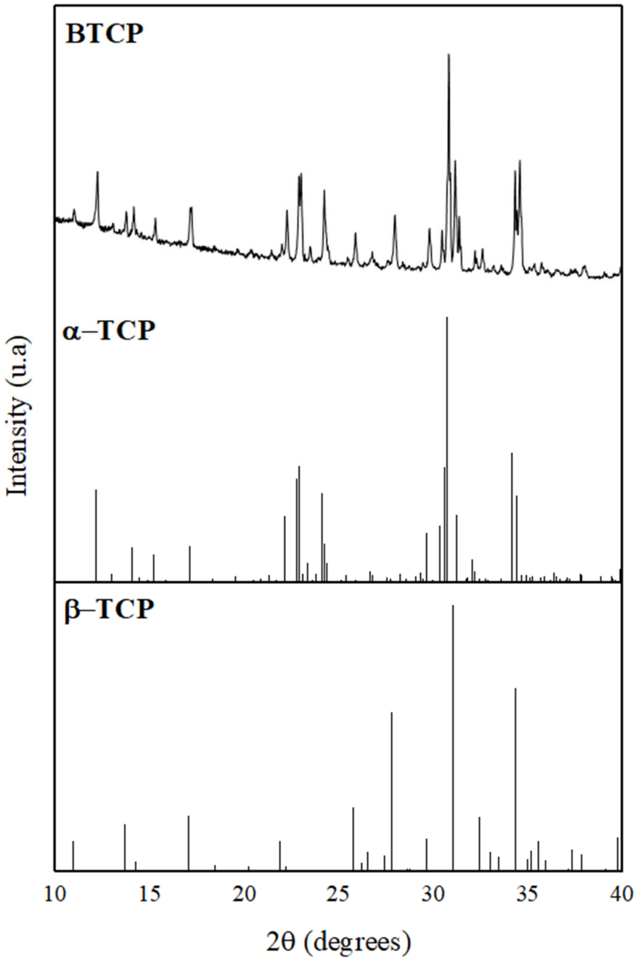

Figure 19- Diffractogram of the powder resultant from the second calcination. The standard JCDD PDF (codes in Table 5, section 2.2.2) α-TCP and β–TCP are also presented for comparison.

Surprisingly, as it can be seen, the obtained powder is not pure α-TCP, but a mixture of α-TCP and β-TCP, so a biphasic powder. The quantification of these crystalline phases obtained by Rietveld refinement shows that powder presents 70 wt.% of α-TCP and 30 wt.% of β-TCP, which fitting is presented in Figure 20. This means that powder from synthesis V and/or VI after first calcination (Figure 18) should be

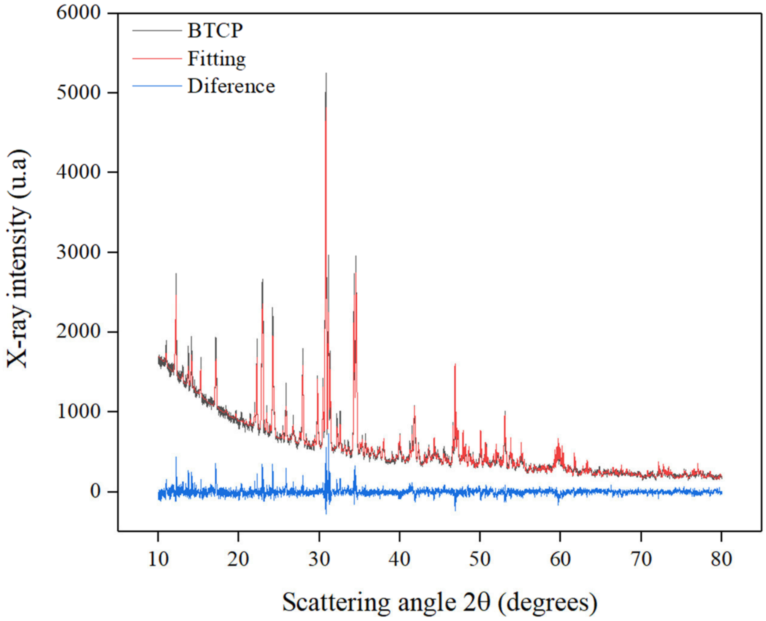

Figure 20- Rietveld refinement used to access the amount of the crystalline phases in the powder resultant from second calcination.

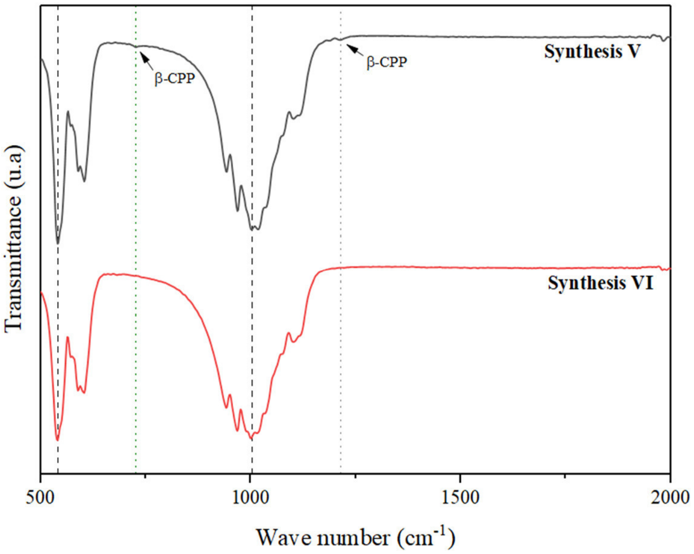

Figure 21 - FTIR spectra of powders resultant from synthesis V and VI (S-V and S-VI) after first thermal treatment.

responsible for the appearance of β-TCP. To clarify this, FTIR has been evaluated in these both powders, which results are presented in Figure 21.

In fact, powder resultant from synthesis V is not only β-TCP as identified by X-Ray diffraction (Figure 19) but present a small amount of β-CPP, only detected by FTIR. The presence of the characteristic vibrational modes of the PO_4 groups (around 550 cm^{-1}, 607 cm^{-1}, 942 cm^{-1}, 970 cm^{-1} and 1042 cm^{-}1) confirm the β-TCP phase formation [139]. The marked bands at 727 cm^{-1} and 1212 cm^{-1} are characteristic of $P_2O_7^{4-}$ group of β-CPP. These bands are clearly visible in the spectrum of S-V and not in S-VI, confirming the existence of traces of β-CPP in S-V, which stabilizes β-TCP phase, explaining the existence of β-TCP phase after the second thermal treatment in the full mixture [95, 127].

From this point forward, the raw powders will be referenced as follows:

- TCP (for β-TCP powder);
- BTCP (for biphasic powder).

PSD analysis was determined using the procedure described in Chapter 2, section 2.2.1. Based on previous works [127], the milling was conducted in a controlled manner. The powders were milled and analyzed for PSD in timed intervals to avoid decreasing the D_{50} particle size below 1 μm. Figure 22 presents particle size distribution of TCP and BTCP powders.

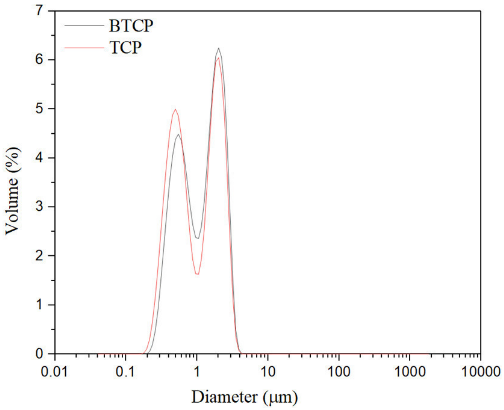

Mixture	**D$_{10}$^{a}**	**D$_{50}$^{b}**	**D$_{90}$^{c}**	**D$_{mean}$^{d}**
TCP	0.38	1.01	2.54	1.29
BTCP	0.43	1.27	2.62	2.07

^{a}**D$_{10}$**: 10% of the total particles are bellow this size;
^{b}**D$_{50}$**: 50% of the total particles are bellow this size;
^{c}**D$_{90}$**:90% of the total particles are bellow this size;
^{d}**D$_{mean}$**: average particle size;

Figure 22- Particle size distribution of the TCP and BTCP powders.

The particle size distribution is one of the most important powder characteristics for cement pastes preparation. Although the particle size distribution mentioned in the previous work (bimodal distribution with D_{50} around 1 μm) was used to obtain injectable cement pastes [127], a similar PSD can be also used to prepare ceramic pastes for molding microneedles. Since the tip of the microneedles ranges form 25-100 μm ideally, reaching a D_{50} around 1-1.5 μm guarantees that this parameter will not influence the molding process. The D_{50} was used as reference parameter to choose when to stop the milling process.

Both TCP and BTCP powders, present a similar bimodal particle size distribution with D_{50} around 1.01 μm and D_{50} around 1.27 μm, respectively. Bimodal particles size distributions are likely to allow the preparation of pastes with highly packing behavior, important factor to avoid high porosity levels and improve the mechanical properties of the final cements [140].

3.2 - Characterization of the cement pastes

Self-setting pastes for casting microneedles molds might follow two important criteria: (1) high initial setting time to allow paste preparation and complete casting and (2) adequate mechanical properties for complete de-molding and skin penetration without damaging. TCP and BTCP cement pastes were tested for its ISTs and FSTs to better understand how an optimization of the molding process could be made. Figure 23 shows the ISTs and FSTs of the cement pastes obtained from TCP and BTCP powders, according to the compositions presented in Table 6 and 7 (Chapter 2).

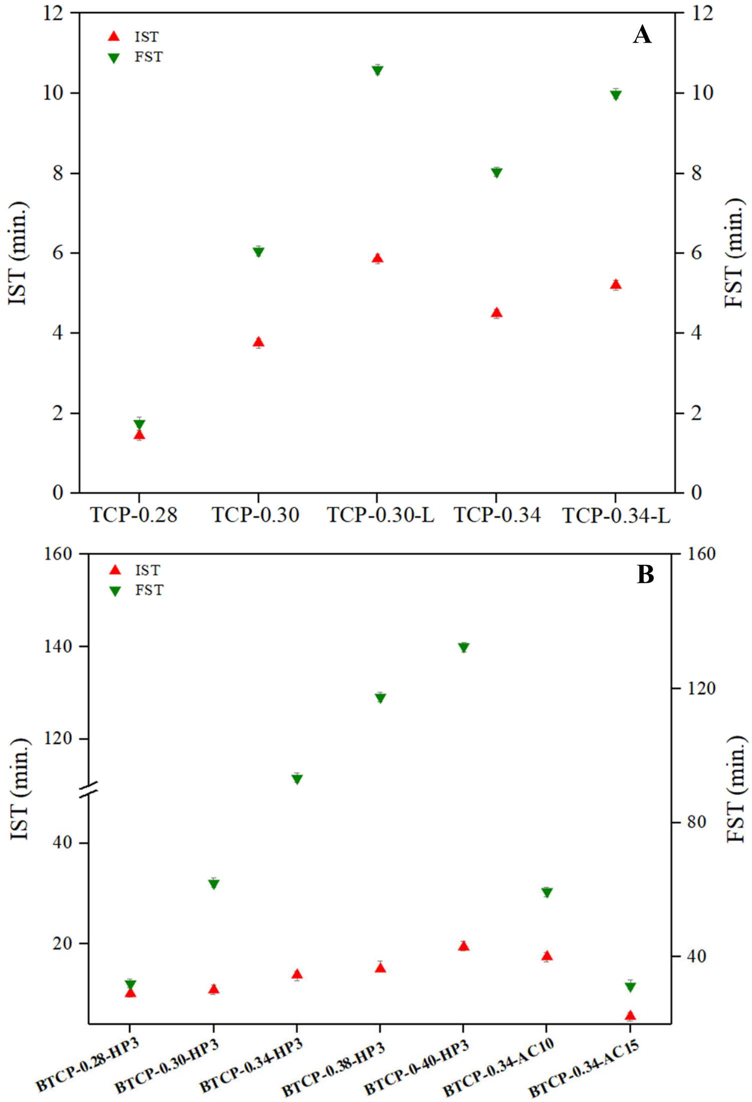

Figure 23 - Initial setting time (IST) and Final setting time (FST) of the cement pastes obtained from TCP (A) and BTCP powders (B), according to the compositions presented in Table 6 and 7 (chapter 2).

For this analysis, the influence of L/P ratio, liquid composition and the addition of levofloxacin in IST and FST were studied for both powders. As expected, as L/P ratio increases, IST and FST increases for both powders [141]. For TCP, IST increases from around 2 min to 5 min when L/P changes from 0.28 to 0.34 while for BTCP, IST increases from 10 min to 20 min when L/P increases from 0.28 to 0.40. For a given L/P ratio, the presence of levofloxacin increases the IST and FST for all cement pastes tested, when compared with the same cements without levofloxacin. These results are in good agreement with results obtained by other authors [141,143].

Comparing the two liquid compositions used in BTCP cement pastes, for the same L/P ratio (0.34) is possible to observe that IST and FST increases from 14 min to 17 min for 10 % AC solution, but decreases to 6 min for 15% AC solution. Adding higher amounts of AC (from 10 to 15 wt %) in aqueous solution, IST and FST decreases. Since for 15 wt.%, IST is too low (5 min), it means that time for casting the paste in the mould will be short to guarantee flowing conditions of the paste to the deeper parts of the mould. Due to that, 10 wt.% of AC solution was used for further studies and the remaining compositions were discarded.

3.3 - Characterization of the CPCs

3.3.1 - Mechanical strength, porosity and crystalline phases

The as-prepared TCP and BTCP cement pastes were molded into cylinders and its mechanical properties tested following the methodology described in section 2.3.2. Compressive strength (A), porosity (B) and crystalline phases (C) of TCP (Figure 24) and BTCP (Figure 26) cement samples, in presence and in the absence of antibiotic, dried in different conditions, were tested. Figure 25 and Figure 27 present the XRD of the resultant cements from TCP and BTCP powders, respectively.

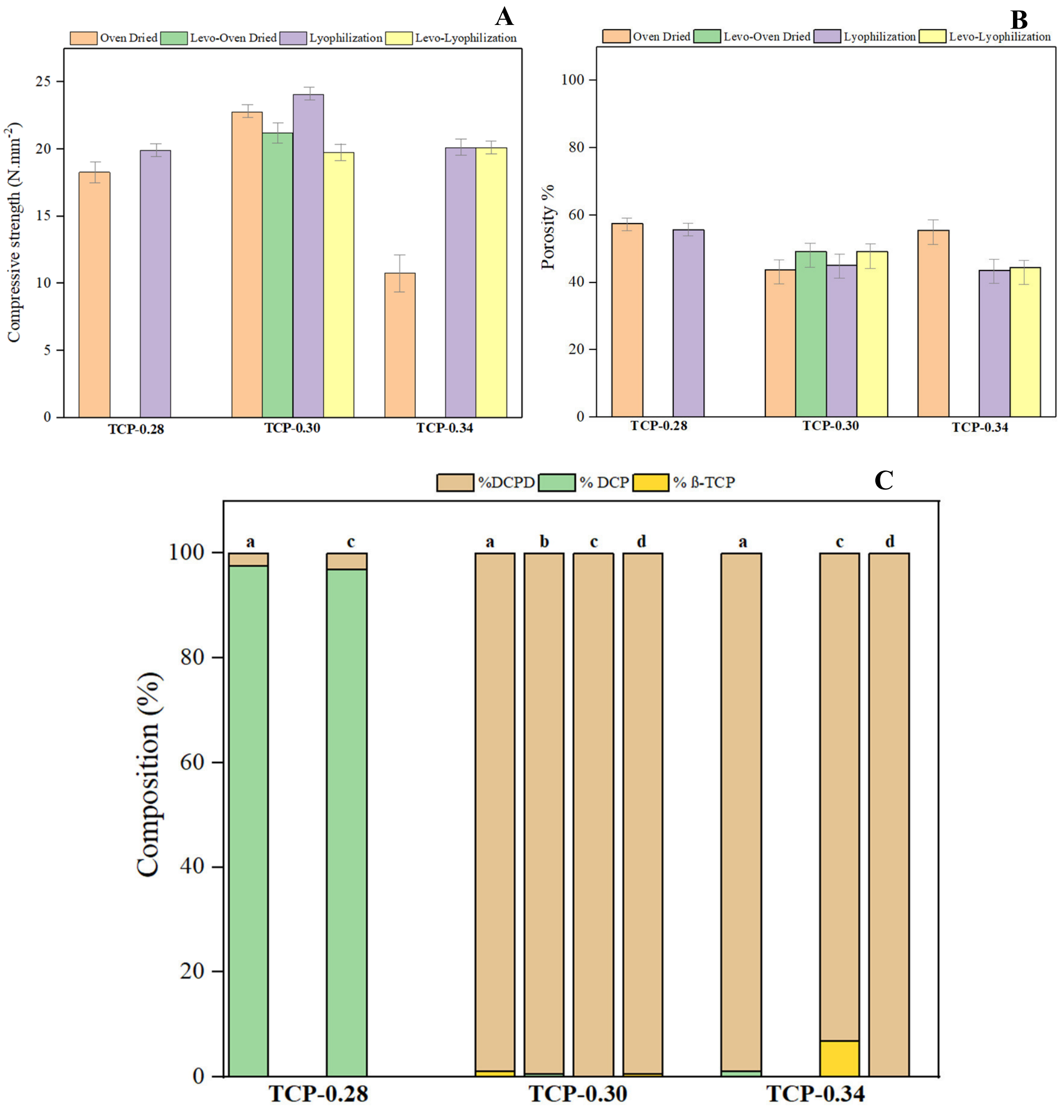

Figure 24- Compressive strength (**A**) total porosity (**B**) and crystalline phases (**C**) of the TCP samples submitted to oven drying (TCP-0.28-OD, TCP-0.30-OD, TCP-0.34-OD) and lyophilization without levofloxacin (TCP-0.28-Liof, TCP-0.30-Liof and TCP-0.34-Liof) and with levofloxacin (TCP-0.30-L-Liof, TCP-0.34-L-Liof). In figure **C**, **a** refers to oven dried, **b** to oven dried + 2.5 wt.% levofloxacin, **c** to lyophilized and **d** to lyophilized samples + 2.5 wt.% levofloxacin.

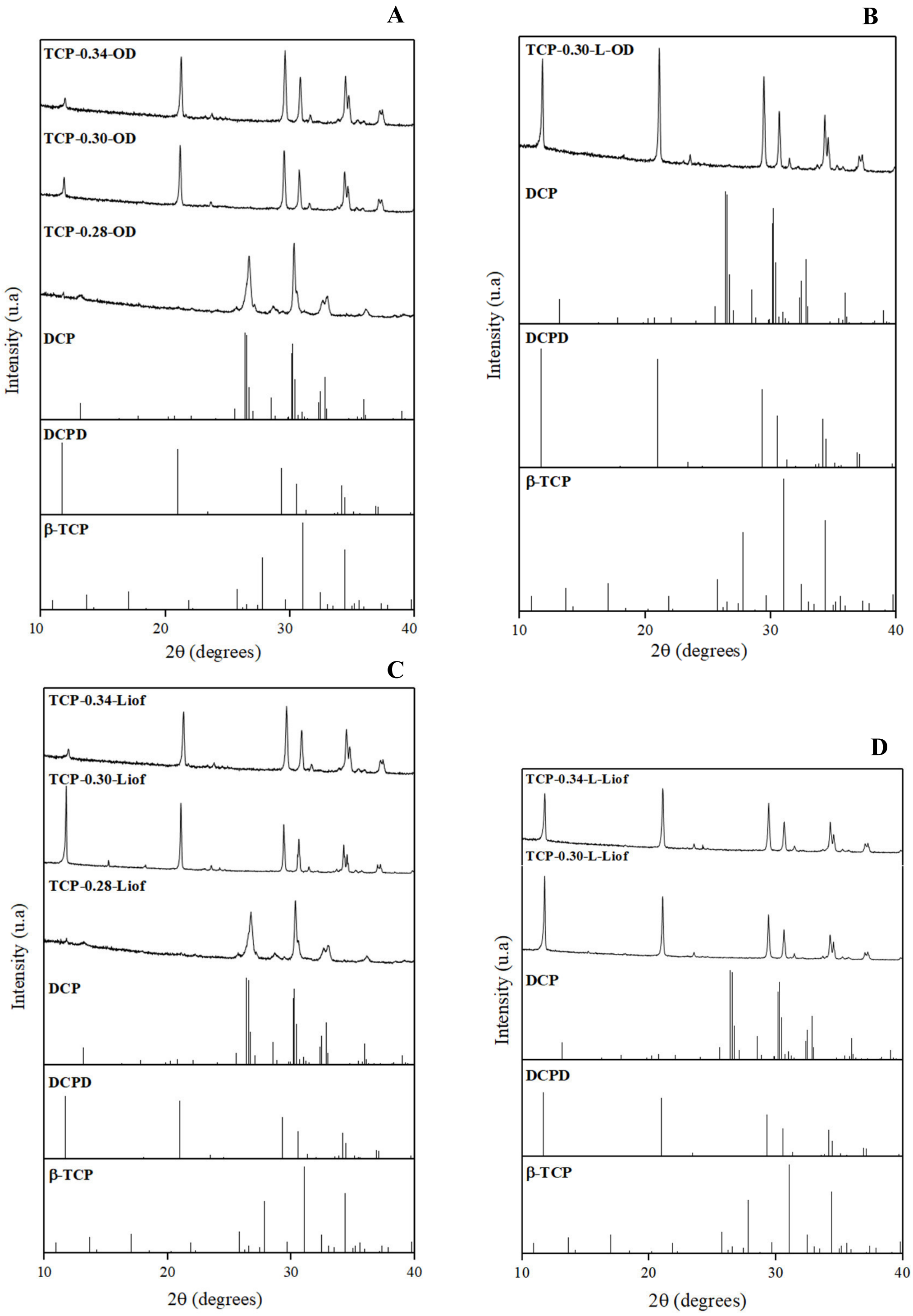

Figure 25 - Diffractogram for TCP samples for oven drying (**A**), oven drying + 2.5% levofloxacin (**B**), lyophilization (**C**) and 2.5% levofloxacin + lyophilization (**D**).

As shown in previous works [127], the mechanical properties and the porosity of the CPCs are tightly related. As the porosity of a sample increases, its mechanical strength should decrease, and vice versa. Moreover, compressive strength of cements increases as L/P ratio decreases with concomitant decreasing of porosity. This trend was verified when L/P ratio changes from 0.30 to 0.34 mL.g^{-1}, instead for 0.28 mL.g^{-1} (Figure 24A) when compared with higher L/P ratios. It can be attributed to: (i) higher viscosity of the pastes for 0.28 mL.g^{-1}L/P ratio, which difficult the casting procedure with subsequent air bubbles trapped in the cement paste; (ii) DCP as crystalline phase formed, which presents lower density than brushite phase.

As it can be seen, drying samples by lyophilization increased the overall compressive strength in all tested TCP samples when compared to the oven dried samples. These results are in good agreement with porosity data (Figure 24B), since a lower porosity increases the mechanical strength of the cement. For 0.30 mLg^{-1} L/P ratio, the addition of levofloxacin decreases the compressive strength of the cements (oven dried and lyophilized), with concomitant increase in porosity values, while for 0.34 mLg^{-1} L/P ratio, slightly variations in both properties were observed. This could be explained by the incomplete transformation of β-TCP in brushite (DCPD) phase (Figure 24C and Figure 25) for the TCP-0.34-liof in absence of levofloxacin.

For cements obtained from BTCP powders, increasing L/P ratio resulted in an expected decrease in compressive strength for the cement samples prepared with aqueous solution containing 3 wt.% HP (Figure 26A The porosity results (Figure 26B) for the BTCP samples indicate that using sodium hydrogen phosphate instead of citric acid results in similar porosity values for the same L/P ratio (0.34). Increasing citric acid concentration from 10 to 15-wt% decreases compressive strength values with a simultaneous increase of porosity. Since citric acid acts like an accelerator of the setting reaction (Figure 23B), viscosity of the cement paste increases rapidly and consequently handling time decreases. Due to that, casting procedure is difficult (likely to air bubbles formation), particles arrangement becomes more difficult resulting in a highly porous structure.

According to the results obtained for TCP cements, addition of levofloxacin slightly decreases compressive strength, as well as, increases porosity.

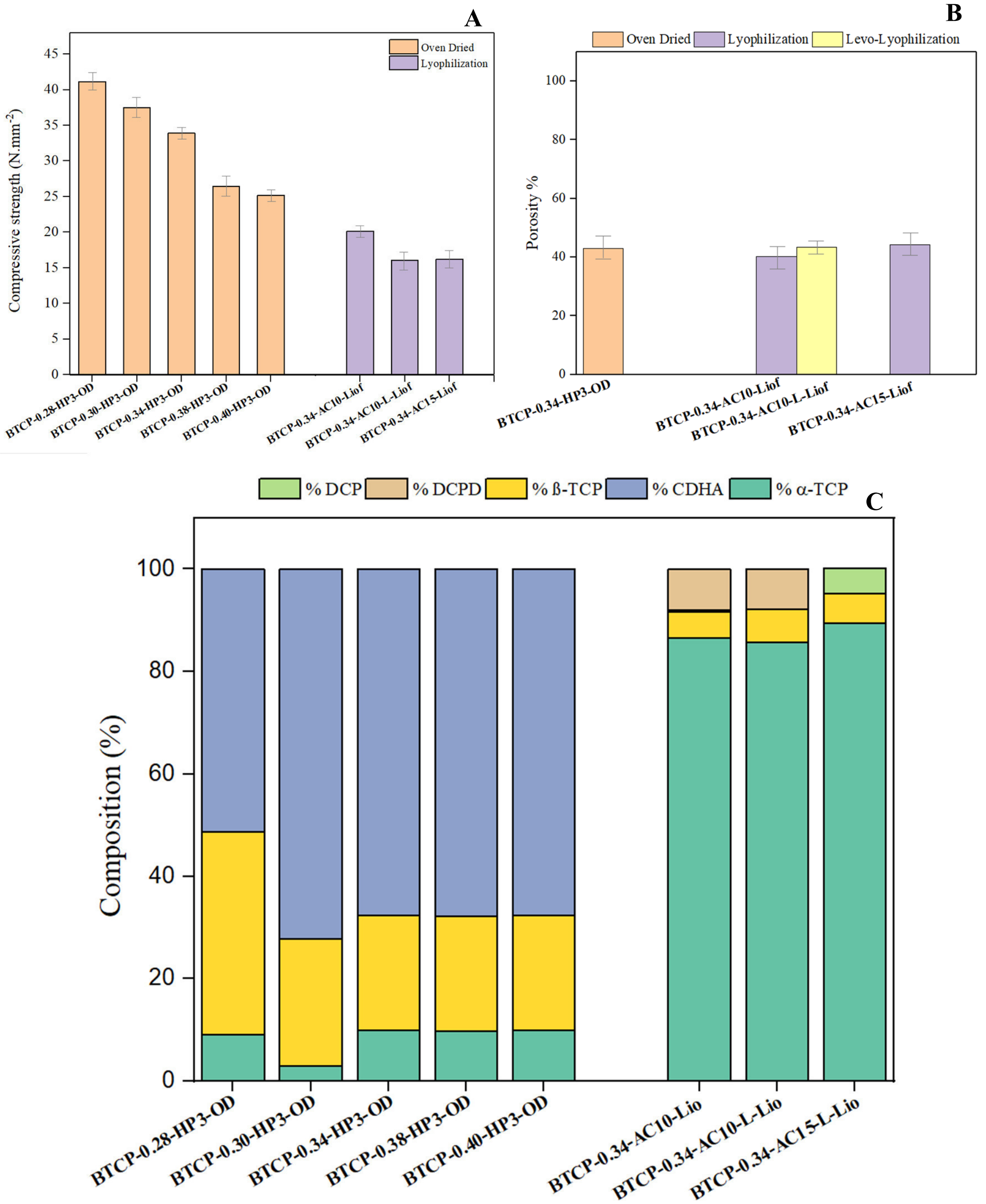

Figure 26- Compressive strength (**A**), porosity (**B**) and crystalline phases (**C**) of the BTCP samples submitted to oven drying and lyophilization and with a fixed liquid phase of hydrogen phosphate and 10% and 15% citric concentration.

The cement compositions were analyzed via XRD in order to identify the converted crystalline phases.

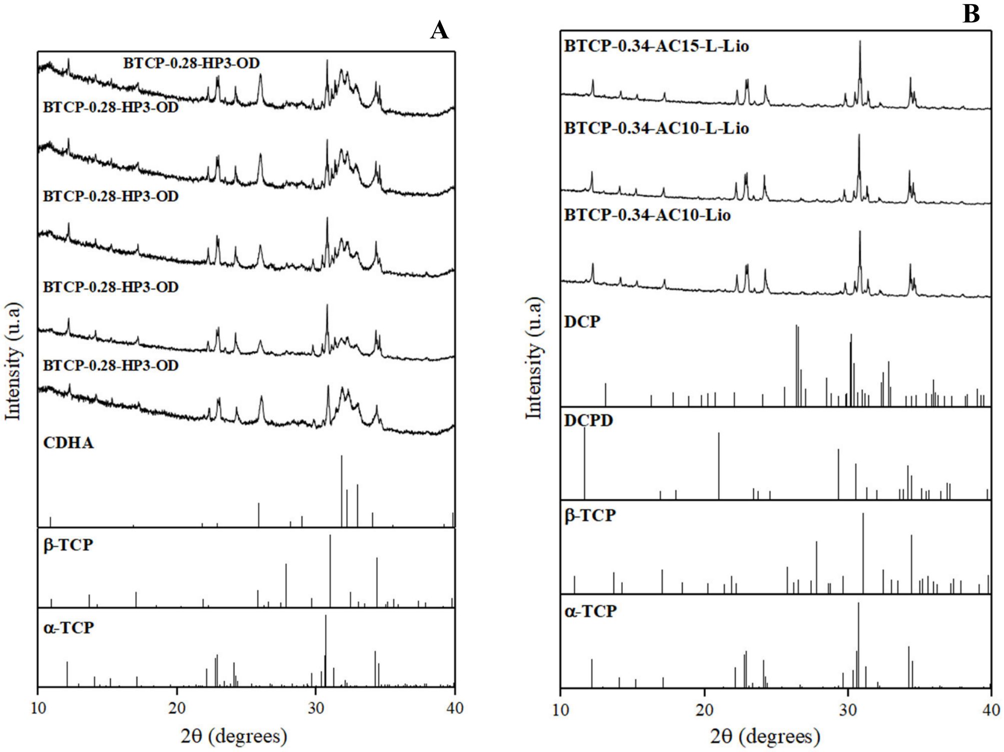

Figure 27- Diffractograms of the BTCP samples, for hydrogen phosphate (**A**) and citric acid (**B**).

For the BTCP samples (Figure 26C and Figure 27) prepared with HP liquid, CDHA is the main phase with unreacted α-TCP and β-TCP. In presence of AC as liquid phase, cements from BTCP powders present unreacted α-TCP as the main phase with small amounts of brushite for BTCP-0.34-10AC in absence or in presence of levofloxacin. For cement prepared with 15-wt% citric acid, monetite (DCP) was formed instead of brushite. This can be attributed both to the lower setting times and pH values of the cement paste.

The differences in the phases composition between BTCP cements prepared with HP and AC as liquid composition, explain the higher compressive strength values obtained for the cement samples prepared with HP. In fact, BTCP-0.34-HP3-OD and BTCP-0.34-AC10-Liof cement samples present similar porosity values while compressive strength of the first is around 34 MPa, significantly higher value than the second one (around 18 MPa). The higher compressive strength is related to the higher amount of CDHA (apatitic phase) in BTCP-0.34-HP3-OD.

Comparing brushitic (Figure 24) and apatitic cements (Figure 26), as for example TCP-0.34-Liof and BTCP-0.34-HP3-OD, similar porosity values can be observed while compressive strength is significantly higher for the apatitic one, as expected.

3.3.2 - Surface analysis

The microstructural characteristics (surface) of the CPCs obtained from TCP powders, i. e., TCP-0.30-L-OD, TCP-0.30-OD, TCP-0.30-L-Liof, TCP-0.30-Liof, TCP-0.34-L-Liof and TCP-0.34-Liof are presented in Figure 28. Figure 29 presents the micrographs of the BTCP-0.34-L-Liof and BTCP-0.34-Liof cements.

The large spherical pores shown in Figure 28 are most likely due to air bubbles trapped in the cement paste during mixing and molding. Analyzing surface microstructures of the TCP cements obtained from 0.30 mL.g^{-1} L/P ratio (Figure 28), oven dried and lyophilized, is possible to observe that lyophilized samples presented a smooth surface with apparently less porosity, in good agreement with compressive strength values for lyophilized samples (Figure 24A). Since total porosity values are similar for oven dried and lyophilized samples (Figure 24B), pore size and size distribution should be different, i.e., lyophilized samples should present small pores homogenously distributed, which could explain the better mechanical properties obtained for lyophilized TCP cements (Figure 24A). The presence of levofloxacin seems to decrease the crystals size, more visible in lyophilized TCP samples prepared with 0.34 mL.g^{-1}.

For the BTCP samples (Figure 29), the presence of levofloxacin appears to increase porosity on the surface with larger pore size, in concordance with the results presented in Figure 26 A and B.

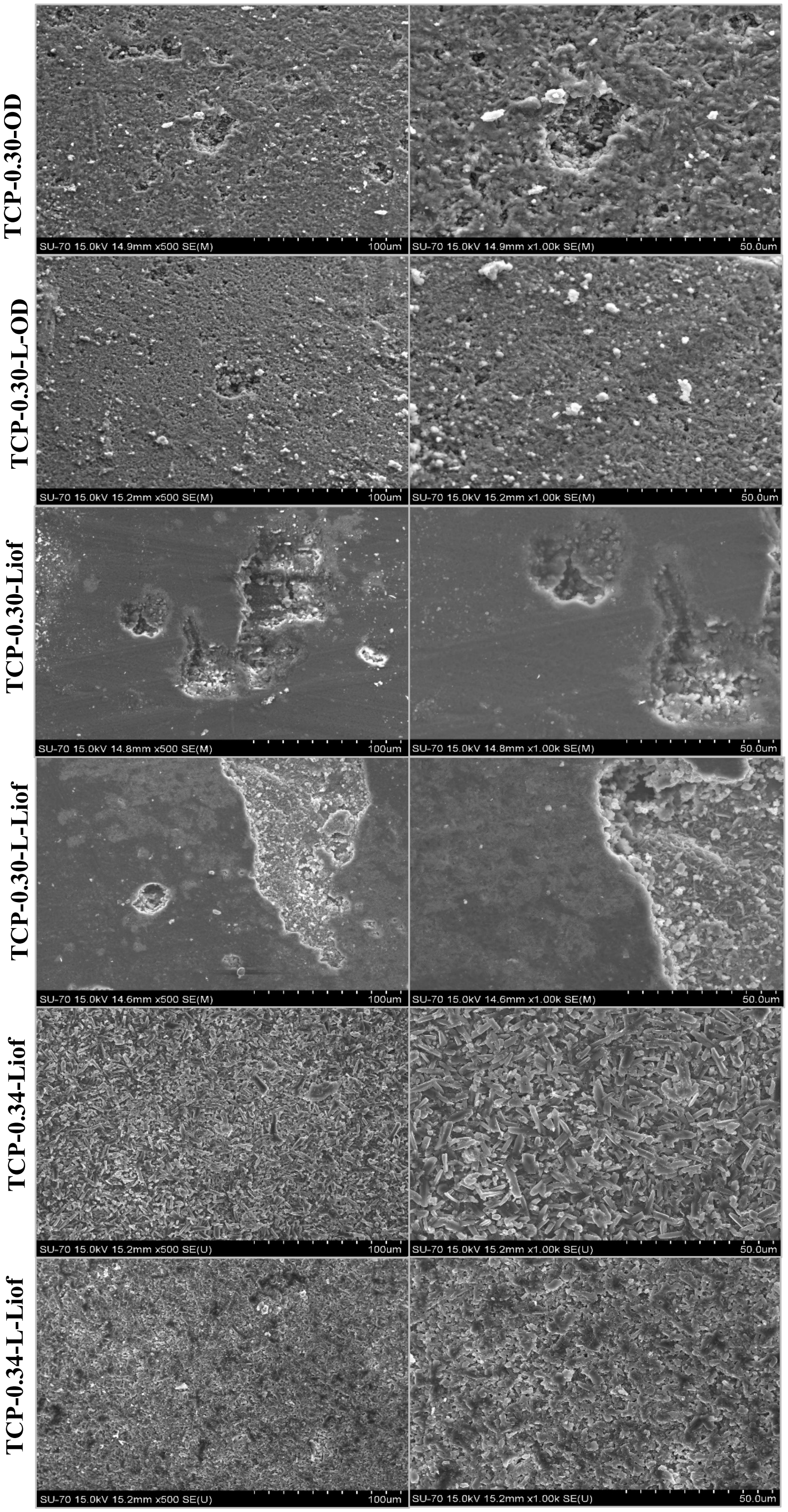

Figure 28 – Surface SEM images of the TCP samples (TCP-0.30-OD, TCP-0.30-Liof, TCP-0.34-Liof) with and without levofloxacin.

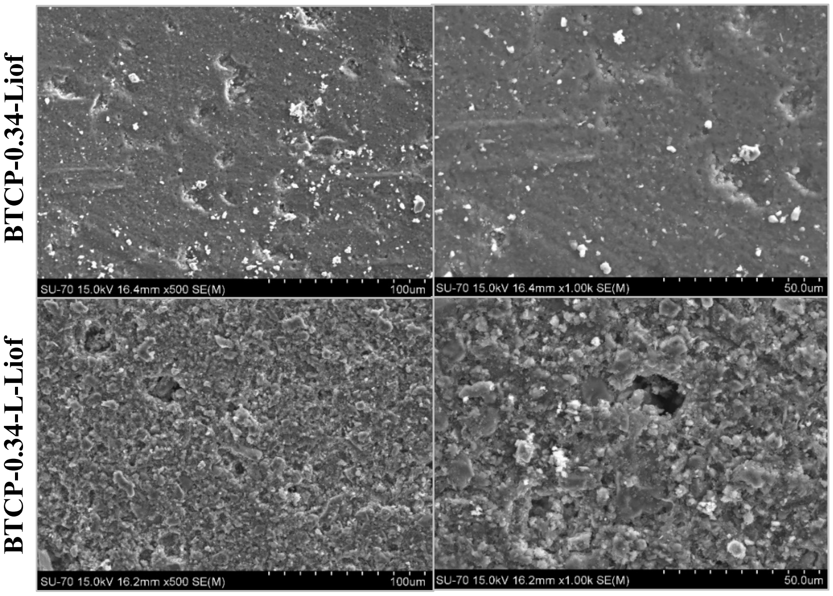

Figure 29- Surface SEM images of the BTCP samples (BTCP-0.34-liof) with and without levofloxacin.

3.4 - Antibiotic release studies

3.4.1 - Quantification method

Calibration curves (and their respective equations) were calculated for each time point (see table in figure 30), and illustrated in Figure 30: Linearity (5-75 µg mL^{-1}) and reproducibility were analyzed and considered adequate for sample analysis, with a coefficient value (C_V/%) of 0.005 > C_V > 0.251.

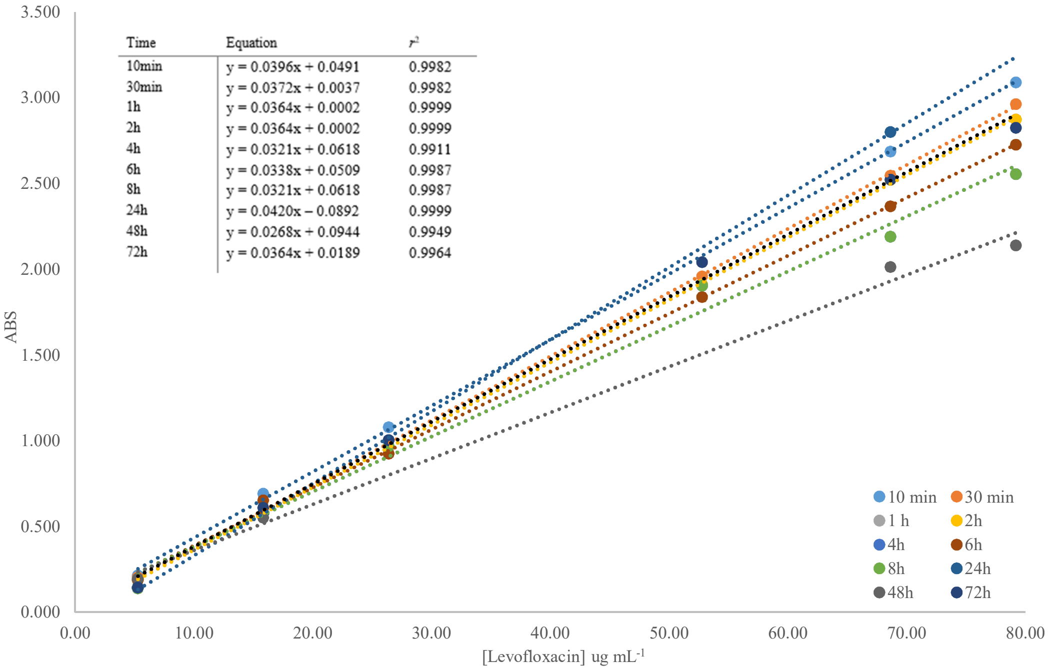

Time	Equation	r^2
10min	$y = 0.0396x + 0.0491$	0.9982
30min	$y = 0.0372x + 0.0037$	0.9982
1h	$y = 0.0364x + 0.0002$	0.9999
2h	$y = 0.0364x + 0.0002$	0.9999
4h	$y = 0.0321x + 0.0618$	0.9911
6h	$y = 0.0338x + 0.0509$	0.9987
8h	$y = 0.0321x + 0.0618$	0.9987
24h	$y = 0.0420x - 0.0892$	0.9999
48h	$y = 0.0268x + 0.0944$	0.9949
72h	$y = 0.0364x + 0.0189$	0.9964

Figure 30 - Calibration curves for each time point and their respective equations and coefficient of determination (r^2).

Clearly, as shown in Figure 30 by the decreasing slope, there was some degradation of the levofloxacin in the media over the 72h period. Comparing the curves with the highest concentration (75.00 µg mL^{-1}) between the 10 min and 48h time points, a decrease of 30.79 % over this period suggests that not only light, but also temperature, influence the stability of the levofloxacin in the solution and therefore, the levofloxacin released by the samples as well. Nevertheless, the effect of temperature is compensated as the concentration of the drug in the release media was calculated using the levofloxacin standard incubated during the same time frame.

3.4.2 - In-vitro drug release

Figure 31 presents release profiles of levofloxacin from the 4 batches studied (table 8, chapter 2, section 2.4.2). As it can be seen, a complete levofloxacin release was achieved for TCP-0.30-L-Liof, TCP-0.30-L-OD and TCP-0.34-L-Liof after 48h and, for BTCP-0.34-L-Liof , after 24h (Figure 31B). The drying process had no influence over the levofloxacin release, as TCP-0.30-L-Liof and TCP-0.30-L-OD present similar cumulative percentage values at all time points (Fig.31 and Table 9).

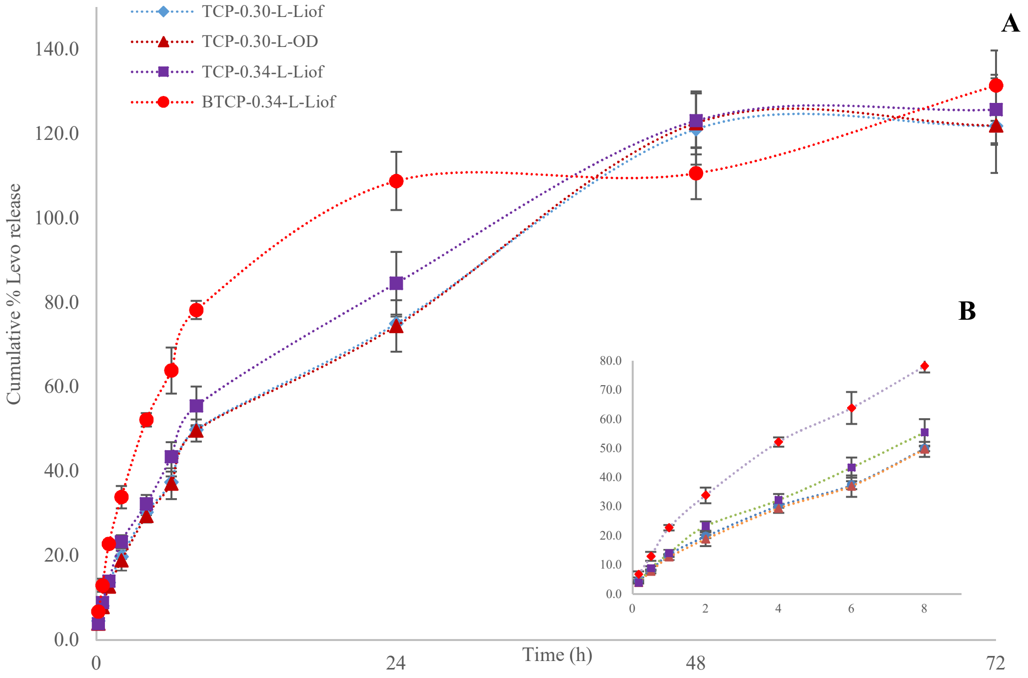

Figure 31- *In vitro* release profiles of the different cement formulations tested (A) and zoom of fig. 31 for the first 8h (B). Markers and error bars represent mean ± SD (n=3). A percentage above 100% is shown in the xx axis to better represent all the obtained data.

Between TCP-0.30-L-Liof and TCP-0.34-L-Liof, a faster release profile for TCP-0.34-L-Liof indicates that L/P has some influence over the release rate. Levofloxacin release increased 9.6% in 24 h, from 75.0 ± 1.6% (TCP-0.30-L-Liof) to 84.6 ± 7.4% (TCP-0.34-L-Liof). BTCP-0.34-L-Liof presents the fastest release profile, with 108.8 ± 6.9% of levofloxacin release over a 24h period.

Table 9 - Cumulative % of levofloxacin released from formulations TCP-0.30-L-Liof (**1**) and TCP-0.30-L-OD (**2**). Mean ± SD (n=3).

	10min	30min	1h	2h	4h	6h	8h	24h	48h
1	4.6 ±0.3%	8.2 ± 0.2%	13.6 ± 0.1%	19.8 ± 0.6%	30.3 ± 0.7%	37.4 ± 1.4%	49.9 ± 0.8%	75.0 ± 1.6 %	121.1 ± 8.5%
2	4.0 ± 0.2%	7.9 ± 0.6%	12.7 ± 0.9%	18.9 ± 2.4%	29.5 ± 1.5%	37.1 ± 3.7%	49.7 ± 2.6%	74.5 ± 6.1%	122.5 ± 7.5 %

3.4.5 - Kinetics

The release kinetic mechanism was obtained with the experimental release data fitted to different kinetic models including: First order; Higuchi and Coupled mechanism [144] (Table 9). For all the formulations, at least half of the levofloxacin content was released in the first 8 hours, even with some major differences between them. Using the Higuchi model for that period, we can observe that the α-TCP (BTCP-0.34-L-Liof) has a higher k_H than the β-TCP formulations, indicating a higher initial release rate. Moreover, the good fit of release data to the Higuchi model (during the first 8h) suggests that the drug is released by simple diffusion mechanism within this initial time frame (Bettencourt et al., 2000). Overall, the best fitting model for all samples was the designated "coupled mechanism", first described by Frutos et al. [145] and previously used to describe other *in vitro* release studies of drugs from bone cements [146,147]. The model, defined in the third equation on Table 10, suggests a mechanism based on dissolution/diffusion process with an initial burst effect. The term $b(1 - e^{-kcmt})$ is associated with a first order kinetic dissolution process and the term $c\sqrt{t}$ with Fickian diffusion. The *b* and *c* parameters represent the contributions (in percentage values) of the dissolution and diffusion processes to the release of levofloxacin at any *t* time, and the parameter *a* is associated with the initial burst effect. The *b* and *c* parameters varied inversely, with the dissolution parameter (parameter *b*) prevailing over the diffusion (parameter *c*) process for all samples (Fig. 32), while the parameter *a* in BTCP-0.34-L-Liof suggests a stronger initial burst release over the other three formulations. As so, on the first 8 hours, due to the higher concentration of levofloxacin in the samples *vs.* the medium, the diffusion process prevails. As the equilibrium is reached, the dissolution process controls the rate at which the levofloxacin is released within the 72 hours.

Table 10- Fitted parameter values and r^2 for the different equation models used to determine the release kinetics of levofloxacin in CaPs TCP-0.30-L-OD (**1**), TCP-0.30-L-Liof (**2**), TCP-0.34-L-Liof (**3**) and BTCP-0.34-L-Liof (**4**).

Equation models	Model parameters	Formulations			
		1	2	3	4
First order	k_1 (h^{-1})	0.001	0.001	0.002	0.003
$L_t = 1 - e^{-k1t}$	r^2	0.9982	0.9983	0.9982	0.9978
Higuchi (8h)	k_H ($h^{-1/2}$)	0.5089	0.5089	0.551	0.7239
$L_t = k_H \sqrt{t}$	r^2	0.9862	0.9845	0.9893	0.9978
Coupled mechanism	a	0.3087	0.2072	0	6.4022
$L_t = a + b\,(1 - e^{-kcmt}) + c\sqrt{t}$	b	73.178	153.40	25.029	104.89
	c (h^{-1})	1.784	1.722	1.804	0
	r^2	0.9982	0.9983	0.9982	0.9978

L_t denotes fraction of levofloxacin released at a given time t. k_1 and k_H are constants of the mathematical models; **a** represents the burst effect, **b** is related with the dissolution process and **c** with the diffusion process of the "coupled mechanism" model.

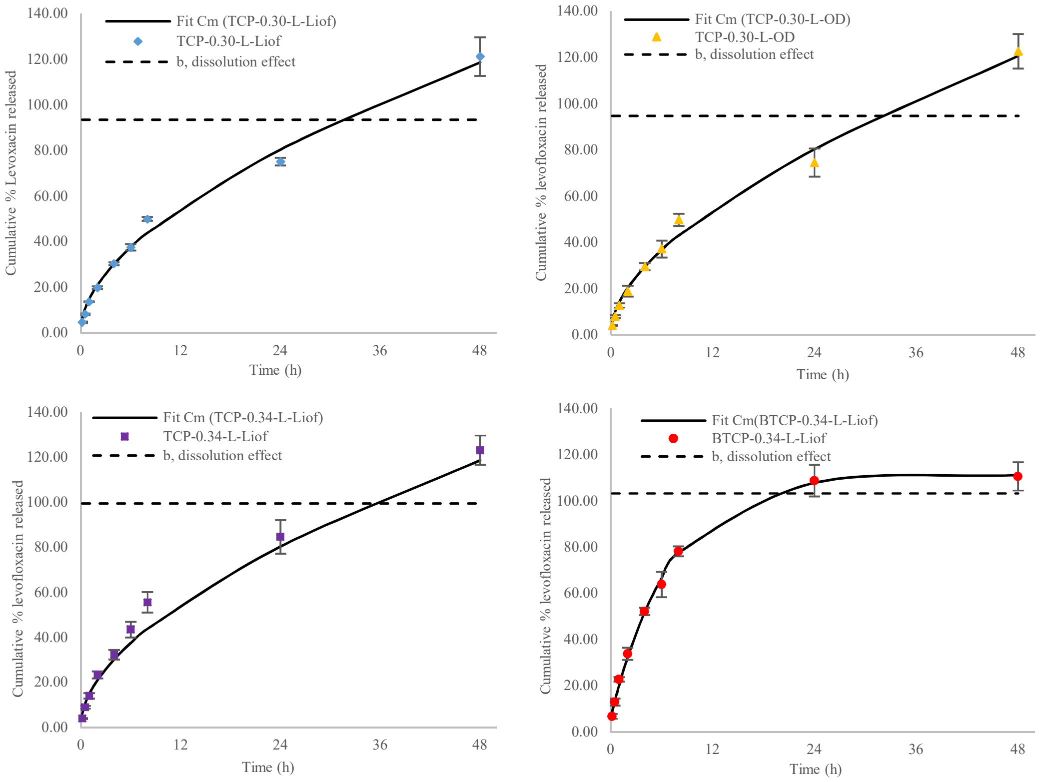

Figure 32 -Levofloxacin release fitted curves with the "coupled mechanism" with the parameter of the model equation presented.

3.5 - Evaluation of levofloxacin distribution throughout cement samples

Raman spectra of the microneedle plates was used to access the distribution of the levofloxacin in oven dried and lyophilized samples. Both sides of the array were analyzed. The bottom side refers to the side without microneedles while top side refers to the side of MN plate (containing the microneedles). Figure 33 presents the Raman spectra obtained in both sides of MN plates for a TCP based MN obtained with 0.34 mLg^{-1} L/P ratio, oven dried and lyophilized, as well as, BTCP based microneedle obtained with the same L/P ratio and dried in both conditions. As expected, all samples presents CaP bands visible at 970 cm^{-1} [139] and levofloxacin bands at 1395 cm^{-1}, 1614 cm^{-1}, 1726 cm^{-1}[148, 149]. Since this analysis is qualitative, it is only possible to extrapolate conclusions within the same sample, by comparing the CaP and levofloxacin intensity bands ratio (most intense ones). However, comparing the Raman spectra obtained in top and bottom sides of TCP-0.34-L-OD and TCP-0.34-L-Liof based MN is difficult to observe significant differences and to draw reliable conclusions.

In order to shed light on this point, Raman confocal images were also obtained in both sides of the MN plates, which are presented in Figure 34 and 35 for, TCP-0.34-L (OD and Liof) and BTCP-0.34-L (OD and Liof), respectively.

Looking to the TCP samples (Figure 34), it seems that the lyophilized samples benefit from this drying procedure, as the drug distribution seems to be more homogenous than in the oven dried samples. On the other hand, the results from the BTCP samples are quite ambiguous, being difficult to draw any firm conclusions concerning the influence of drying process on drug distribution. For that, additional experiments should be evaluated.

Furthermore, since drug release profiles for oven dried and lyophilized samples have been similar (Figure 31), it means that levofloxacin distribution throughout cement samples should be analogous in both drying procedures.

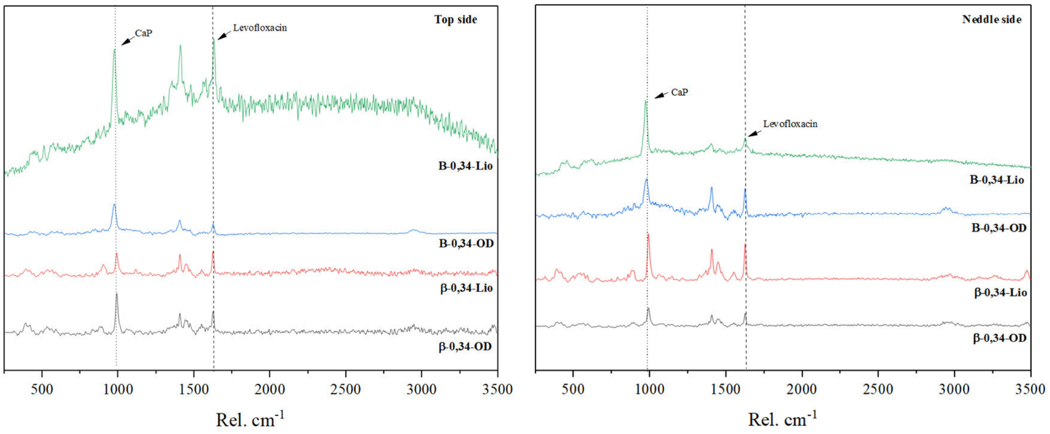

Figure 33 - Raman spectra of the microneedles from both sides of the array, top side (right, with needles) and bottom side (left, without needles).

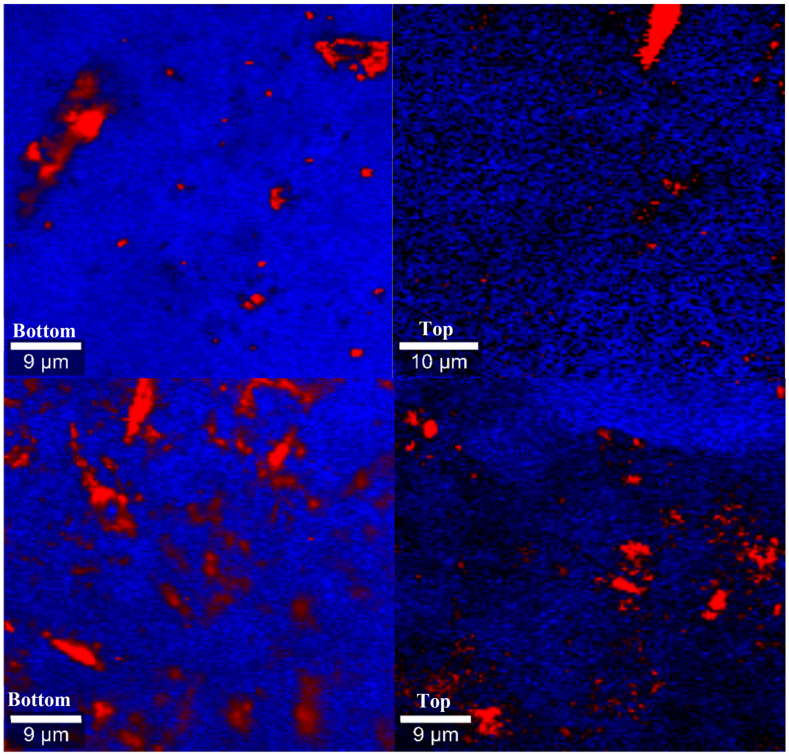

Figure 34- Combined Raman images of TCP-0.34-L-OD (first row) and TCP-0.34-L-Liof (bottom row) samples. Blue corresponds to CaPs and the red to Levofloxacin.

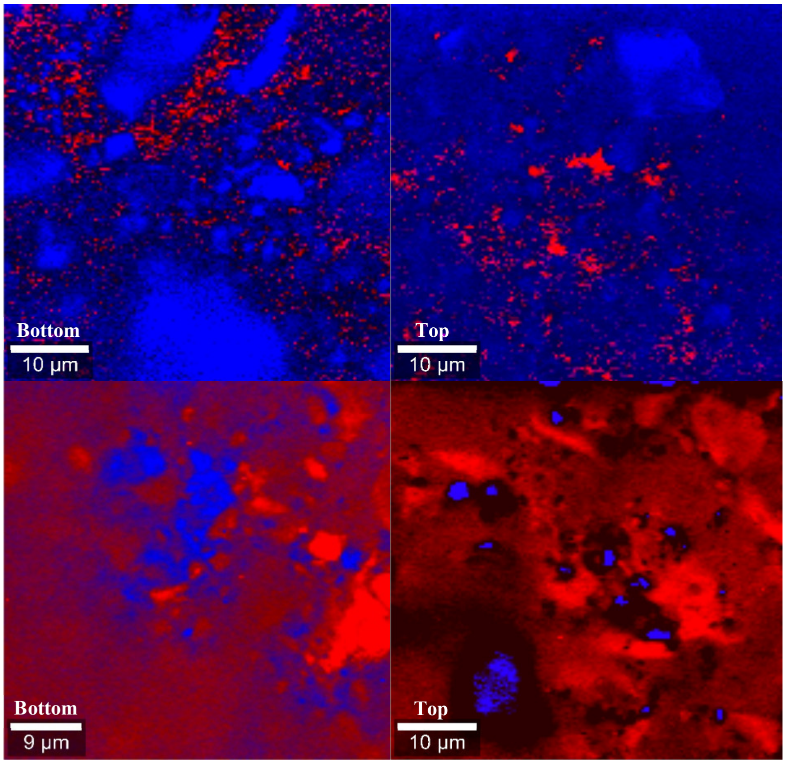

Figure 35 - Combined Raman images of BTCP-0.34-L-OD (first row) and BTCP-0.34-L-Liof (bottom row) samples. Blue corresponds to CaPs and the red to Levofloxacin on the first row, but on the bottom blue is CaP and red is levofloxacin.

3.5 Microneedle characterization

3.5.1 - Mechanical properties and SEM imaging

To have a better perspective of the microneedle array, images of the microneedles were taken using a regular camera (13 MP), a magnifying glass camera (Leica EZ4 HD) and a SEM microscope. SEM imaging (x30, x100 magnifications) was used to characterize microneedles and to measure them, while the other camera was used to acquire images that better represent the arrays. The results are shown in Figures 36-38.

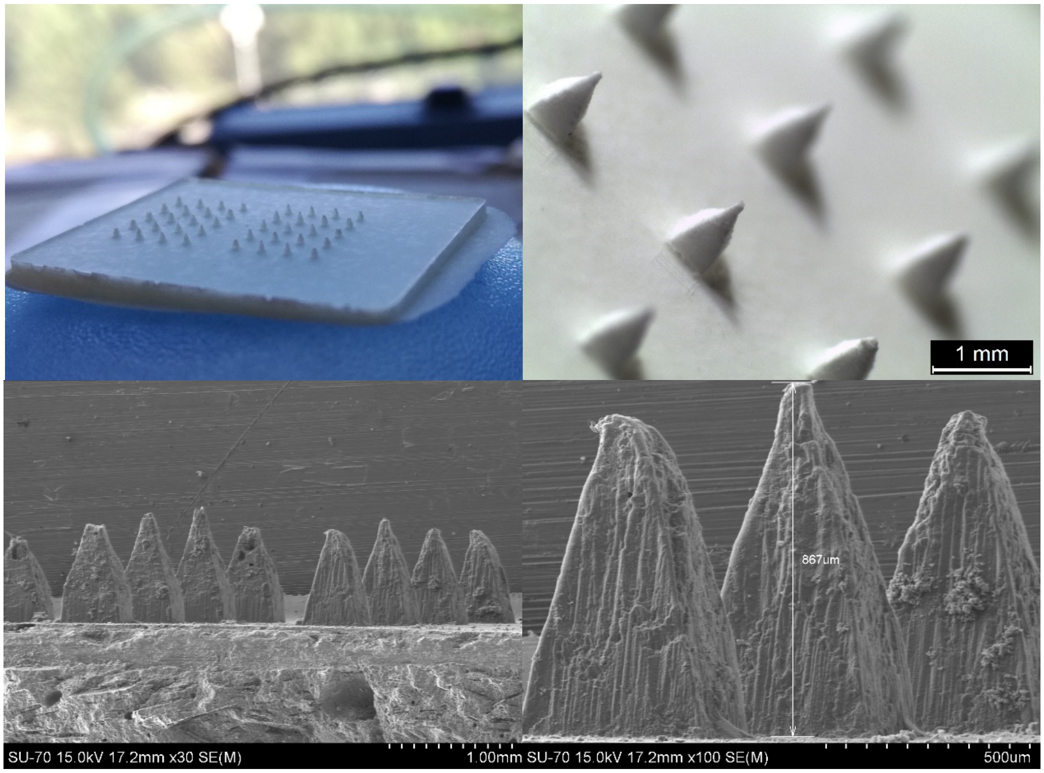

Figure 36- TCP-0.30-L-Liof microneedles. Images taken with camera (top left) a magnifying glass camera (top right) and SEM (bottom) with x30 and x100 magnifications.

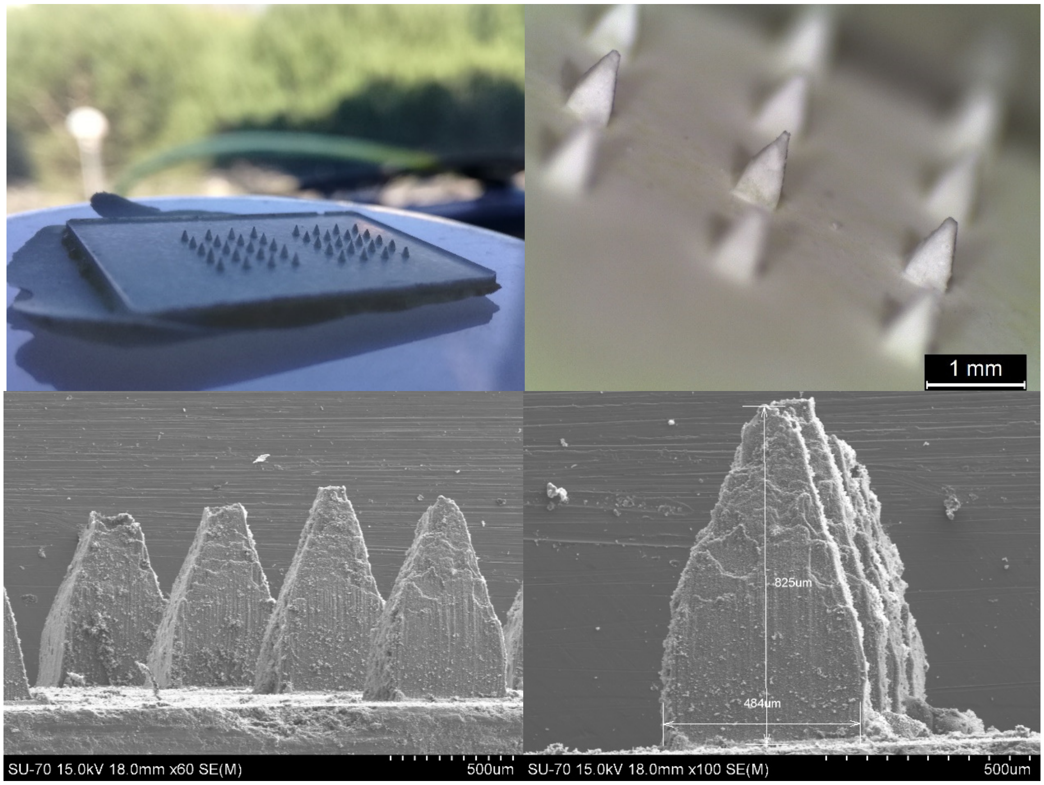

Figure 37 – TCP-0.34-L-Liof microneedles. Images taken with camera (top left) a magnifying glass camera (top right) and SEM (bottom) with x30 and x100 magnifications.

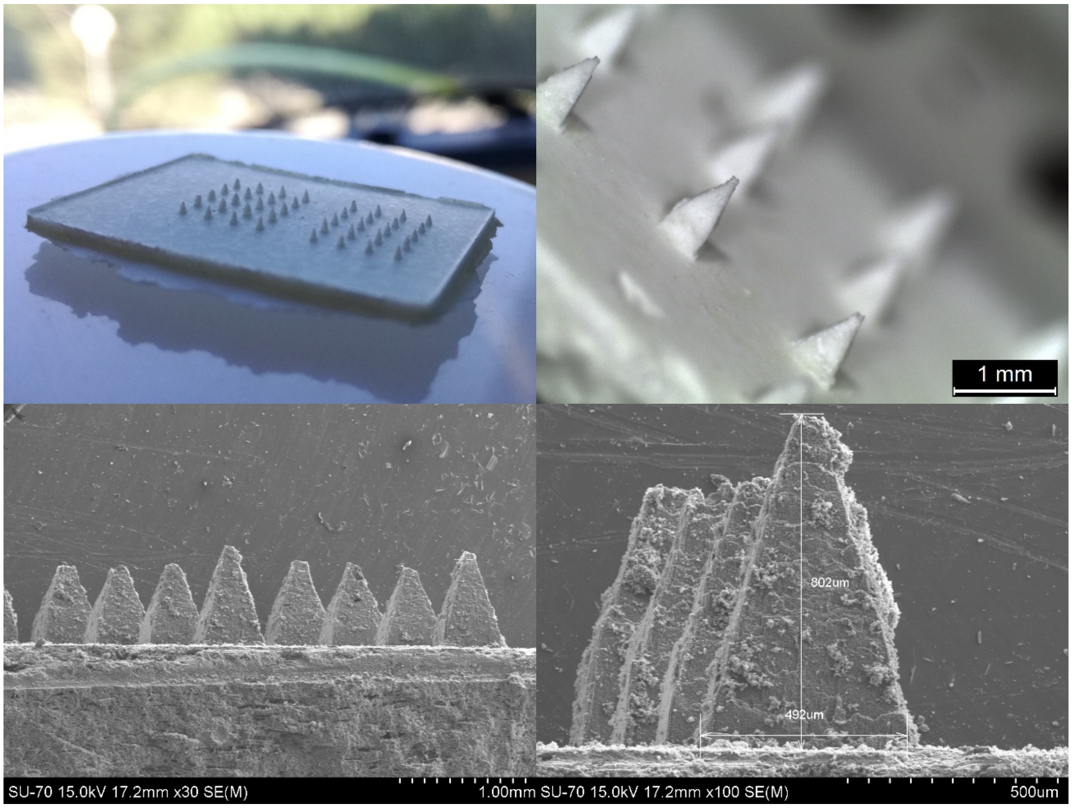

Figure 38 - BTCP-0.34-L-Liof microneedles. Images taken with camera (top left) a magnifying glass camera (top right) and SEM (bottom) with x30 and x100 magnification.

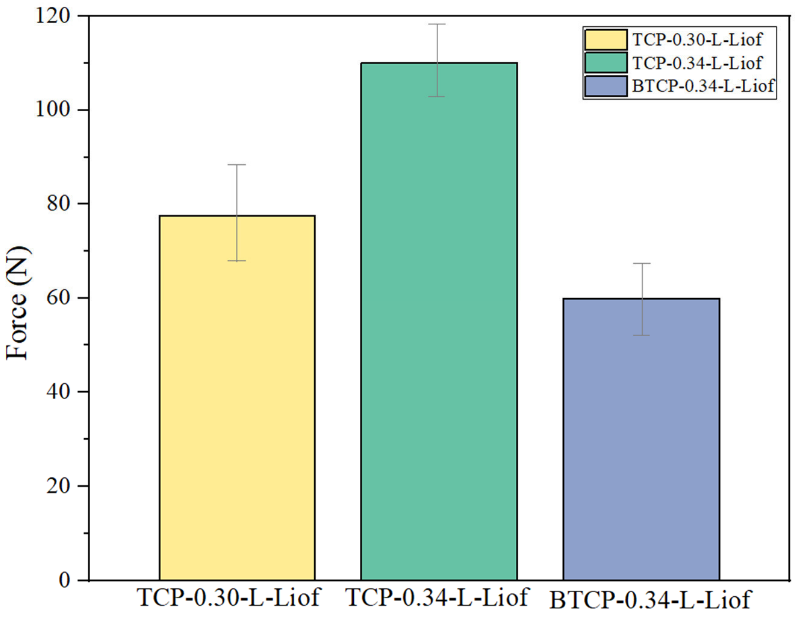

Figure 39- Compressive force of the microneedles.

All the above images show fully filled needle tips and some partially filled. The incomplete filling is derived to the not-yet optimized molding procedure and the PSD not being optimal (> 1 µm), as the larger particles can obstruct deeper parts of the mold (tip of MN). Other mentioned techniques (chapter 2, section 2.5), such as vacuum filling, had slightly worse filling performance for the same needle geometry [141], confirming the manual filling as the best molding method for high viscosity pastes.

The tips of the TCP-0.30-L-Liof, TCP-0.34-L-Liof and BTCP-0.30-Liof and BTCP-0.34-L-Liof based microneedles were tested by compressive test to evaluate the maximum force that can be applied to the MN without damaging the tip. Results are presented in Figure 39. These values should be prudently analyzed since the MN in the array could present different length resultant to the incomplete fill of the MN mold (high standard deviation values). As higher the length of MN, as sharper is the tip resulting in smaller tip surface area and, consequently, lower mechanical resistance. The TCP-0.34-L-Liof composition was the most resistant with 110 N, followed by the TCP-0-30-L-Liof with 77 N and the BTCP-0.34-L-Liof with 57 N.

Comparing these results with the ones obtained by Cai et al. [16], the height of the fabricated needles is 4 times the size of the ones obtained in this study.

Chapter 4:
Conclusions and Future work

4. Conclusions and Future work

With a main objective of producing drug-loaded ceramic microneedles capable of piercing the skin and successfully deliver all of the drug, this thesis can be considered a success, at least on that point. From the obtained results, we can conclude:

- The control of pH and temperature of the synthesis reaction are essential experimental parameters to obtained the desired crystalline phases in CaP based powders;
- The presence of Na_2HPO_4 in liquid phase composition used for the BTCP cements preparation avoids the solubilization of levofloxacin, interfering in the cement setting.
- The L/P ratio influences the mechanical resistances of the cements;
- The addition of levofloxacin increased the setting times of all the tested compositions;
- The addition of levofloxacin slightly decreased the mechanical properties of the cements;
- Drying process by Lyophilization increases the mechanical properties of the resultant cements;
- All the cement based MN tested have enough mechanical strength to pierce the surface of the skin;
- From the release assay, we can conclude that the levofloxacin is 100% released within the first 48 hours, for all compositions tested.

As the microneedles present promising characteristics for future biomedical applications, further work should be done:

- Developing an improved method for casting the microneedles;
- Evaluate skin penetration tests with the self-setting microneedles obtained
- Evaluate the transdermal drug delivery *in situ*.

References

[1] S. V. P. Verma, A.S. Thakur, K. Deshmukh, Dr. A.K. Jha, “Routes of drug administration - Pharmacorama,” *Int. J. Pharm. Stud. Res.*, vol. I, no. I, pp. 54–59, 2010.

[2] A. L. Daugherty and R. J. Mrsny, “Emerging technologies that overcome biological barriers for therapeutic protein delivery,” *Expert Opin. Biol. Ther.*, vol. 3, no. 7, pp. 1071–1081, Oct. 2003.

[3] M. R. Prausnitz and R. Langer, “Transdermal drug delivery,” *Nat. Biotechnol.*, vol. 26, no. 11, pp. 1261–1268, Nov. 2009.

[4] K. van der Maaden, R. Luttge, P. J. Vos, J. Bouwstra, G. Kersten, and I. Ploemen, “Microneedle-based drug and vaccine delivery via nanoporous microneedle arrays,” *Drug Deliv. Transl. Res.*, vol. 5, no. 4, pp. 397–406, Aug. 2015.

[5] S. M. Bal, Z. Ding, E. Van Riet, W. Jiskoot, and J. A. Bouwstra, “Advances in transcutaneous vaccine delivery: Do all ways lead to Rome?,” *Journal of Controlled Release*, vol. 148, no. 3. pp. 266–282, 20-Dec-2010.

[6] J.-F. Nicolas and B. Guy, “Intradermal, epidermal and transcutaneous vaccination: from immunology to clinical practice,” *Expert Rev. Vaccines*, vol. 7, no. 8, pp. 1201–1214, Oct. 2008.

[7] FDA, “FDA approved Transderm Scop in December 1979,” 1979. [Online]. Available: https://www.accessdata.fda.gov/scripts/cder/daf/index.cfm?event=overview.process&ApplNo=017874. [Accessed: 29-Feb-2017].

[8] N. Sharma, G. Agarwal, A. C. Rana, and D. Kumar, “A Review: Transdermal Drug Delivery System: A Tool For Novel Drug Delivery System,” *Int. J. Drug Dev. Res.*, vol. 3, no. 3, pp. 70–84, 2011.

[9] N. Akhtar, “Microneedles : An Innovative approach to Transdermal Delivery - A Review,” *Int. J. Pharm. Pharm. Sci.*, vol. 6, no. 4, pp. 18–25, 2014.

[10] S. Indermun *et al.*, “Current advances in the fabrication of microneedles for transdermal delivery,” *J. Control. Release*, vol. 185, no. 1, pp. 130–138, Jul. 2014.

[11] K. Lee, C. Y. Lee, and H. Jung, “Dissolving microneedles for transdermal drug administration prepared by stepwise controlled drawing of maltose,” *Biomaterials*, vol. 32, no. 11, pp. 3134–3140, Apr. 2011.

[12] T. Omatsu *et al.*, “Metal microneedle fabrication using twisted light with spin,” *Opt. Express*, vol. 18, no. 17, p. 17967, Aug. 2010.

[13] G. Li, A. Badkar, S. Nema, C. S. Kolli, and A. K. Banga, “In vitro transdermal delivery of therapeutic antibodies using maltose microneedles,” *Int. J. Pharm.*, vol. 368, no. 1–2, pp. 109–115, Feb. 2009.

[14] K. Alyamani and C. Bach, “Intravenous Drugs - Microneedle Patches,” *J. Multidiscip. Eng. Sci. Technol.*, vol. 1, no. 5, pp. 53–60, 2014.

[15] S. Bystrova and R. Luttge, “Micromolding for ceramic microneedle arrays,” in *Microelectronic Engineering*, 2011, vol. 88, no. 8, pp. 1681–1684.

[16] B. Cai, W. Xia, S. Bredenberg, and H. Engqvist, “Self-setting bioceramic microscopic protrusions for transdermal drug delivery,” *J. Mater. Chem. B*, vol. 2, no. 36, pp. 5992–5998, Jul. 2014.

[17] S. Cooper, *The Biology of the Skin*, 3rd ed., vol. 95. 2002.

[18] R. R. Wickett and M. O. Visscher, “Structure and function of the epidermal barrier,” *Am. J. Infect. Control*, vol. 34, no. 10 Suppl., 2006.

[19] W. D. (William D. James, T. G. Berger, D. M. Elston, and R. B. Odom, *Andrews' diseases of the skin : clinical dermatology.* Saunders Elsevier, 2006.

[20] Z. Nemes and P. M. Steinert, “Bricks and mortar of the epidermal barrier.,” *Exp. Mol. Med.*, vol. 31, no. 1, pp. 5–19, 1999.

[21] P. M. Elias, “Stratum corneum defensive functions: An integrated view,” *J. Invest. Dermatol.*, vol. 125, no. 2, pp. 183–200, Aug. 2005.

[22] P. M. Elias and E. H. Choi, “Interactions among stratum corneum defensive functions,” *Exp. Dermatol.*, vol. 14, no. 10, pp. 719–726, Oct. 2005.

[23] D. Mohammed, P. J. Matts, J. Hadgraft, and M. E. Lane, “In vitro-in vivo correlation in skin permeation,” *Pharm. Res.*, vol. 31, no. 2, pp. 394–400, Feb. 2014.

[24] G. Kasting and J. Nitsche, “Mathematical Models of Skin Permeability: Microscopic Transport Models and Their Predictions,” in *Computational Biophysics of the Skin*, Pan Stanford Publishing, 2014, pp. 187–216.

[25] T. F. Wang, G. B. Kasting, and J. M. Nitsche, “A multiphase microscopic diffusion model for stratum corneum permeability. I. Formulation, solution, and illustrative results for representative compounds,” *J. Pharm. Sci.*, vol. 95, no. 3, pp. 620–648, Mar. 2006.

[26] S. Hansen, “Development of a physiology based diffusion model to predict dermal absorption using experimental input parameters", Dissertation zur Erlangung des Grades des Doktors der Naturwissenschaften der Naturwissenschaftlich-Technischen Fakultät III Chemie , Pharma, p. 184, 2009.

[27] D. A. Edwards and R. Langer, “A linear theory of transdermal transport phenomena,” *J. Pharm. Sci.*, vol. 83, no. 9, pp. 1315–1334, Sep. 1994.

[28] G. C. Charalambopoulou, P. Karamertzanis, E. S. Kikkinides, a K. Stubos, N. K. Kanellopoulos, and a T. Papaioannou, “A study on structural and diffusion properties of porcine stratum corneum based on very small angle neutron scattering data,” *Pharm. Res.*, vol. 17, no. 9, pp. 1085–91, Sep. 2000.

[29] H. I. M. Robert L. Bronaugh, “Percutaneous Absorption: Drugs, Cosmetics, Mechanisms, Methodology: Drugs - Google Livros,” *CRC Press*, 1999. [Online].Available:https://books.google.pt/books?id=S1KKpigh3OAC&dq=Percutaneous+Absorption:+Mechanisms,+Methodology,+Drug+Delivery%3B+Marcel+Dekker:+New+York,+1989.&hl=pt-PT&source=gbs_navlinks_s. [Accessed: 21-Aug-2017].

[30] S. Park, Y. Hata, O. Ito, K. Tokioka, and K. Kagawa, “Umbilical Reconstruction after Repair of Omphalocele and Gastroschisis,” *Plast. Reconstr. Surg.*, vol. 104, no. 1, pp. 204–207, Jul. 1999.

[31] G. B. Jemec, B. Jemec, B. I. Jemec, and J. Serup, “The effect of superficial hydration on the mechanical properties of human skin in vivo: implications for plastic surgery.,” *Plast. Reconstr. Surg.*, vol. 85, no. 1, pp. 100–3, Jan. 1990.

[32] W. W. Lu, W. Y. Ip, A. D. Holmes, S. P. Chow, and W. M. Jing, “Biomechanical properties of thin skin flap after basic fibroblast growth factor (bFGF) administration,” *Br. J. Plast. Surg.*, vol. 53, no. 3, pp. 225–229, Apr. 2000.

[33] X. Zhao *et al.*, “Cell infiltrative hydrogel fibrous scaffolds for accelerated wound healing,” *Acta Biomater.*, vol. 49, pp. 66–77, Feb. 2017.

[34] C. Edwards, A. Pearse, R. Marks, Y. Nishimori, K. Matsumoto, and M. Kawai, “Degenerative Alterations of Dermal Collagen Fiber Bundles in Photodamaged Human Skin and UV-Irradiated Hairless Mouse Skin: Possible Effect on Decreasing Skin Mechanical Properties and Appearance of Wrinkles,” *J. Invest. Dermatol.*, vol. 117, no. 6, pp. 1458–1463, Dec. 2001.

[35] J. S. Moon and C. H. Oh, “Solar damage in skin tumors: Quantification of elastotic material,” *Dermatology*, vol. 202, no. 4, pp. 289–292, 2001.

[36] J. Schalkwijk, “Cross-Linking of Elafin/SKALP to Elastic Fibers in Photodamaged Skin: Too Much of a Good Thing?,” *J. Invest. Dermatol.*, vol. 127, no. 6, pp. 1286–1287, Jun. 2007.

[37] D. C. Salter, H. C. McArthur, J. E. Crosse, and A. D. Dickens, “Skin mechanics measured in vivo using torsion: a new and accurate model more sensitive to age, sex and moisturizing treatment,” *Int. J. Cosmet. Sci.*, vol. 15, no. 5, pp. 200–218, Oct. 1993.

[38] S. A. Wissing and R. H. Müller, “The influence of solid lipid nanoparticles on skin hydration and viscoelasticity: in vivo study.,” *Eur. J. Pharm. Biopharm.*, vol. 56, no. 1, pp. 67–72, Jul. 2003.

[39] L. Palma, L. T. Marques, J. Bujan, and L. M. Rodrigues, “Dietary water affects human skin hydration and biomechanics,” *Clin. Cosmet. Investig. Dermatol.*, vol. 8, pp. 413–421, Aug. 2015.

[40] H. G. Vogel, “Directional variations of mechanical parameters in rat skin depending on maturation and age.”, *J. Invest. Dermatol.*, vol. 76, no. 6, pp. 493–497, Jun. 1981.

[41] C. Escoffier, J. de Rigal, A. Rochefort, R. Vasselet, J. L. Lévêque, and P. G. Agache, “Age-related mechanical properties of human skin: an in vivo study.”, *J. Invest. Dermatol.*, vol. 93, no. 3, pp. 353–357, Sep. 1989.

[42] X. Liang and S. A. Boppart, “Biomechanical properties of in vivo human skin from dynamic optical coherence elastography”, *IEEE Trans. Biomed. Eng.*, vol. 57, no. 4, pp. 953–959, 2010.

[43] K. V. Larin and D. D. Sampson, “Optical coherence elastography – OCT at work in tissue biomechanics [Invited],” *Biomed. Opt. Express*, vol. 8, no. 2, p. 1172, Feb. 2017.

[44] J. M. Schmitt, “OCT elastography: imaging microscopic deformation and strain of tissue,” *Opt. Express*, vol. 3, no. 6, p. 199, Sep. 1998.

[45] J. Rogowska, “Optical coherence tomographic elastography technique for measuring deformation and strain of atherosclerotic tissues,” *Heart*, vol. 90, no. 5, pp. 556–562, May 2004.

[46] B. F. Kennedy *et al.*, “Optical coherence micro-elastography: mechanical-contrast imaging of tissue microstructure,” *Biomed. Opt. Express*, vol. 5, no. 7, p. 2113, Jul. 2014.

[47] R. K. Wang, Z. Ma, and S. J. Kirkpatrick, “Tissue Doppler optical coherence elastography for real time strain rate and strain mapping of soft tissue,” *Appl. Phys. Lett.*, vol. 89, no. 14, p. 144103, Oct. 2006.

[48] M. Razani, A. Mariampillai, C. Sun, T. W. H. Luk, V. X. D. Yang, and M. C. Kolios, “Feasibility of optical coherence elastography measurements of shear wave propagation in homogeneous tissue equivalent phantoms,” *Biomed. Opt. Express*, vol. 3, no. 5, p. 972, May 2012.

[49] S. Wang and K. V. Larin, “Optical coherence elastography for tissue characterization: A review,” *J. Biophotonics*, vol. 8, no. 4, pp. 279–302, Apr. 2015.

[50] D. P. Wermeling *et al.*, “Microneedles permit transdermal delivery of a skin-impermeant medication to humans,” *Proc. Natl. Acad. Sci.*, vol. 105, no. 6, pp. 2058–2063, Feb. 2008.

[51] S. P. Davis, B. J. Landis, Z. H. Adams, M. G. Allen, and M. R. Prausnitz, “Insertion of microneedles into skin: Measurement and prediction of insertion force and needle fracture force,” *J. Biomech.*, vol. 37, no. 8, pp. 1155–1163, Aug. 2004.

[52] R. F. Donnelly *et al.*, “Optical coherence tomography is a valuable tool in the study of the effects of microneedle geometry on skin penetration characteristics and in-skin dissolution,” *J. Control. Release*, vol. 147, no. 3, pp. 333–341, Nov. 2010.

[53] A. M. Römgens, D. L. Bader, J. A. Bouwstra, F. P. T. Baaijens, and C. W. J. Oomens, “Monitoring the penetration process of single microneedles with varying tip diameters,” *J. Mech. Behav. Biomed. Mater.*, vol. 40, pp. 397–405, Dec. 2014.

[54] K. Van Der Maaden, W. Jiskoot, and J. Bouwstra, “Microneedle technologies for (trans)dermal drug and vaccine delivery,” *J. Control. Release*, vol. 161, no. 2, pp. 645–655, Jul. 2012.

[55] T. M. Tuan-Mahmood *et al.*, “Microneedles for intradermal and transdermal drug delivery,” *European Journal of Pharmaceutical Sciences*, vol. 50, no. 5. pp. 623–637, 18-Dec-2013.

[56] M. R. Prausnitz, “Microneedles for transdermal drug delivery,” *Adv. Drug Deliv. Rev.*, vol. 56, no. 5, pp. 581–587, Mar. 2004.

[57] D. V. McAllister *et al.*, “Microfabricated needles for transdermal delivery of macromolecules and nanoparticles: Fabrication methods and transport studies,” *Proc. Natl. Acad. Sci.*, vol. 100, no. 24, pp. 13755–13760, Nov. 2003.

[58] R. F. Donnelly, T. R. R. Singh, and A. D. Woolfson, “Microneedle-based drug delivery systems: Microfabrication, drug delivery, and safety,” *Drug Deliv.*, vol. 17, no. 4, pp. 187–207, May 2010.

[59] J. H. Oh *et al.*, “Influence of the delivery systems using a microneedle array on the permeation of a hydrophilic molecule, calcein,” *Eur. J. Pharm. Biopharm.*, vol. 69, no. 3, pp. 1040–1045, Aug. 2008.

[60] S. M. Olhero, E. Lopes, and J. M. F. Ferreira, “Fabrication of ceramic microneedle: The role of specific interactions between processing additives and the surface of oxide particles in Epoxy Gel Casting,” *J. Eur. Ceram. Soc.*, vol. 36, no. 16, pp. 4131–4140, Dec. 2016.

[61] X. H. M. Hartmann, P. Van Der Linde, E. F. G. A. Homburg, L. C. A. Van Breemen, A. M. De Jong, and R. Luttge, "Insertion process of ceramic nanoporous microneedles by means of a novel mechanical applicator design," *Pharmaceutics*, vol. 7, no. 4, pp. 503–522, Nov. 2015.

[62] A. K. Banga, "Microporation applications for enhancing drug delivery," *Expert Opin. Drug Deliv.*, vol. 6, no. 4, pp. 343–354, Apr. 2009.

[63] M. Cormier *et al.*, "Transdermal delivery of desmopressin using a coated microneedle array patch system," *J. Control. Release*, vol. 97, no. 3, pp. 503–511, Jul. 2004.

[64] Z. Ding *et al.*, "Microneedle arrays for the transcutaneous immunization of diphtheria and influenza in BALB/c mice," *J. Control. Release*, vol. 136, no. 1, pp. 71–78, May 2009.

[65] F. J. Verbaan *et al.*, "Improved piercing of microneedle arrays in dermatomed human skin by an impact insertion method," *J. Control. Release*, vol. 128, no. 1, pp. 80–88, May 2008.

[66] S. Aoyagi, H. Izumi, Y. Isono, M. Fukuda, and H. Ogawa, "Laser fabrication of high aspect ratio thin holes on biodegradable polymer and its application to a microneedle," *Sensors Actuators, A Phys.*, vol. 139, no. 1–2 SPEC. ISS., pp. 293–302, Sep. 2007.

[67] F. Pérennès, B. Marmiroli, M. Matteucci, M. Tormen, L. Vaccari, and E. Di Fabrizio, "Sharp beveled tip hollow microneedle arrays fabricated by LIGA and 3D soft lithography with polyvinyl alcohol," *J. Micromechanics Microengineering*, vol. 16, no. 3, pp. 473–479, Mar. 2006.

[68] P. G. Jung *et al.*, "Nickel Microneedles Fabricated by Sequential Copper and Nickel Electroless Plating and Copper Chemical Wet Etching," *Sensors Mater.*, vol. 20, no. 1, pp. 45–53, 2008.

[69] H. Becker and C. Gärtner, "Polymer microfabrication technologies for microfluidic systems," *Anal. Bioanal. Chem.*, vol. 390, no. 1, pp. 89–111, Jan. 2008.

[70] D. C. Duffy, J. C. McDonald, O. J. A. Schueller, and G. M. Whitesides, “Rapid prototyping of microfluidic systems in poly(dimethylsiloxane),” *Anal. Chem.*, vol. 70, no. 23, pp. 4974–4984, 1998.

[71] H. Selvaraj, B. Tan, and K. Venkatakrishnan, “Maskless direct micro-structuring of PDMS by femtosecond laser localized rapid curing,” *J. Micromechanics Microengineering*, vol. 21, no. 7, p. 75018, Jul. 2011.

[72] X. H. M. Hartmann, P. Van Der Linde, E. F. G. A. Homburg, L. C. A. Van Breemen, A. M. De Jong, and R. Luttge, “Insertion process of ceramic nanoporous microneedles by means of a novel mechanical applicator design,” *Pharmaceutics*, vol. 7, no. 4, pp. 503–522, Nov. 2015.

[73] E. M. M. Lopes, “Microagulhas cerâmicas para libertação controlada de fármacos,” 2014.

[74] C. H. Chin, A. Muchtar, C. H. Azhari, M. Razali, and M. Aboras, “Optimization of pH and dispersant amount of Y-TZP suspension for colloidal stability,” *Ceram. Int.*, vol. 41, no. 8, pp. 9939–9946, 2015.

[75] J. F. Kelso and T. A. Ferrazzoli, “Effect of Powder Surface Chemistry on the Stability of Concentrated Aqueous Dispersions of Alumina,” *J. Am. Ceram. Soc.*, vol. 72, no. 4, pp. 625–627, Apr. 1989.

[76] M. Peymannia, A. Soleimani-Gorgani, M. Ghahari, and M. Jalili, “The effect of different dispersants on the physical properties of nano $CoAl_2O_4$ ceramic ink-jet ink,” *Ceram. Int.*, vol. 41, no. 7, pp. 9115–9121, 2015.

[77] S. V. Dorozhkin and M. Epple, “Biological and medical significance of calcium phosphates,” *Angewandte Chemie - International Edition*, vol. 41, no. 17. pp. 3130–3146, 02-Sep-2002.

[78] M. Bohner, “Calcium orthophosphates in medicine: From ceramics to calcium phosphate cements,” *Injury*, vol. 31, no. Suppl. 4. pp. D37–D47, 2000.

[79] B. Boonchom, “Parallelogram-like microparticles of calcium dihydrogen phosphate monohydrate ($Ca(H_2PO_4)_2{\cdot}H_2O$) obtained by a rapid precipitation route in aqueous and acetone media,” *J. Alloys Compd.*, vol. 482, no. 1–2, pp. 199–202, Aug. 2009.

[80] S. V. Dorozhkin, "Calcium orthophosphate cements and concretes," *Materials (Basel).*, vol. 2, no. 1, pp. 221–291, Mar. 2009.

[81] J. C. Elliott, "General chemistry of the calcium orthophosphates," *Stud. Inorg. Chem.*, vol. 18, no. C, pp. 1–62, 1994.

[82] B. Dickens, L. W. Schroeder, and W. E. Brown, "Crystallographic studies of the role of Mg as a stabilizing impurity in β-$Ca_3(PO_4)_2$. The crystal structure of pure β-Ca3(PO4)2," *J. Solid State Chem.*, vol. 10, no. 3, pp. 232–248, Jul. 1974.

[83] M. Mathew, L. W. Schroeder, B. Dickens, and W. E. Brown, "The crystal structure of α-$Ca_3(PO_4)_2$," *Acta Crystallogr. Sect. B Struct. Crystallogr. Cryst. Chem.*, vol. 33, no. 5, pp. 1325–1333, May 1977.

[84] M. Kitamura, C. Ohtsuki, H. Iwasaki, S. I. Ogata, M. Tanihara, and T. Miyazaki, "The controlled resorption of porous β-tricalcium phosphate using a hydroxypropylcellulose coating," *J. Mater. Sci. Mater. Med.*, vol. 15, no. 10, pp. 1153–1158, Oct. 2004.

[85] C. L. Camiré, U. Gbureck, W. Hirsiger, and M. Bohner, "Correlating crystallinity and reactivity in an α-tricalcium phosphate," *Biomaterials*, vol. 26, no. 16, pp. 2787–2794, Jun. 2005.

[86] M. Bohner, R. Luginbühl, C. Reber, N. Doebelin, G. Baroud, and E. Conforto, "A physical approach to modify the hydraulic reactivity of α-tricalcium phosphate powder," *Acta Biomater.*, vol. 5, no. 9, pp. 3524–3535, Nov. 2009.

[87] C. L. Camiré, P. Nevsten, L. Lidgren, and I. McCarthy, "The effect of crystallinity on strength development of α-TCP bone substitutes," *J. Biomed. Mater. Res. - Part B Appl. Biomater.*, vol. 79, no. 1, pp. 159–165, Oct. 2006.

[88] M.-P. Ginebra, E. Fernández, F. C. M. Driessens, and J. A. Planell, "Modeling of the Hydrolysis of α-Tricalcium Phosphate," *J. Am. Ceram. Soc.*, vol. 82, no. 10, pp. 2808–2812, Dec. 2004.

[89] R. G. Carrodeguas, A. H. De Aza, X. Turrillas, P. Pena, and S. De Aza, "New approach to the β→α polymorphic transformation in magnesium-substituted tricalcium phosphate and its practical implications," *J. Am. Ceram. Soc.*, vol. 91, no. 4, pp. 1281–1286, Apr. 2008.

[90] E. B. Montufar, Y. Maazouz, and M. P. Ginebra, “Relevance of the setting reaction to the injectability of tricalcium phosphate pastes,” *Acta Biomater.*, vol. 9, no. 4, pp. 6188–6198, Apr. 2013.

[91] J. T. Zhang, F. Tancret, and J. M. Bouler, “Fabrication and mechanical properties of calcium phosphate cements (CPC) for bone substitution,” *Mater. Sci. Eng. C*, vol. 31, no. 4, pp. 740–747, May 2011.

[92] R. Enderle, F. Götz-Neunhoeffer, M. Göbbels, F. A. Müller, and P. Greil, “Influence of magnesium doping on the phase transformation temperature of β-TCP ceramics examined by Rietveld refinement,” *Biomaterials*, vol. 26, no. 17, pp. 3379–3384, Jun. 2005.

[93] M. Bohner, J. Lemaitre, A. P. Legrand, J.-B. D ’espinose De, L. Caillerie, and P. Belgrand, “Synthesis, X-ray diffraction and solid-state 31^{P} magic angle spinning NMR study of a-tricalcium orthophosphate,” *Materials (Basel).*, vol. 7, no. 7, pp. 457–463, Jul. 1996.

[94] J. H. Welch and W. Gutt, “High-temperature studies of the system calcium oxide–phosphorus pentoxide,” *J. Chem. Soc.*, vol. 0, no. 0, pp. 4442–4444, Jan. 1961.

[95] P. M. C. Torres *et al.*, “Influence of Mg-doping, calcium pyrophosphate impurities and cooling rate on the allotropic α↔β-tricalcium phosphate phase transformations,” *J. Eur. Ceram. Soc.*, vol. 36, no. 3, pp. 817–827, Feb. 2016.

[96] A. Destainville, E. Champion, D. Bernache-Assollant, and E. Laborde, “Synthesis, characterization and thermal behavior of apatitic tricalcium phosphate,” *Mater. Chem. Phys.*, vol. 80, no. 1, pp. 269–277, Apr. 2003.

[97] A. M. J. Lemaitre, A. Mirtchi, “Calcium phosphate cements for medical use: state of the art and perspectives of development.,” *Silic. Ind.*, vol. 52, no. 9–10, pp. 141–146, 1987.

[98] H. L. R. Alves, L. A. dos Santos, and C. P. Bergmann, “Injectability evaluation of tricalcium phosphate bone cement,” *J. Mater. Sci. Mater. Med.*, vol. 19, no. 5, pp. 2241–2246, May 2008.

[99] B. D. Ratner and A. S. Hoffman, *Non-Fouling Surfaces*, vol. 5, no. 3. Academic Press, 2013.

[100] Brown W.E., Chow L.C., “Dental restorative cement pastes.,” 1985.

[101] B. Han *et al.*, “β-TCP/MCPM-based premixed calcium phosphate cements,” *Acta Biomater.*, vol. 5, no. 8, pp. 3165–3177, Oct. 2009.

[102] F. C. M. Driessens, “Calcium phosphates and ceramics bone cements vs. acrylic cements,” *An. Química*, vol. 93, no. 93, pp. S38–S43, 1997.

[103] S. V Dorozhkin, “Calcium orthophosphates: occurrence, properties, biomineralization, pathological calcification and biomimetic applications.,” *Biomatter*, vol. 1, no. 2. Taylor & Francis, pp. 121–164, 2011.

[104] A. A. Mirtchi, J. Lemaitre, and N. Terao, “Calcium phosphate cements: study of the β-tricalcium phosphate - monocalcium phosphate system,” *Biomaterials*, vol. 10, no. 7, pp. 475–480, Sep. 1989.

[105] M. Bohner, P. Van Landuyt, H. P. Merkle, and J. Lemaitre, “Composition effects on the pH of a hydraulic calcium phosphate cement,” *J. Mater. Sci. Mater. Med.*, vol. 8, no. 11, pp. 675–681, Nov. 1997.

[106] B. R. Constantz *et al.*, “Histological, chemical, and crystallographic analysis of four calcium phosphate cements in different rabbit osseous sites,” *J. Biomed. Mater. Res.*, vol. 43, no. 4, pp. 451–461, 1998.

[107] M. Bohner, “Reactivity of calcium phosphate cements,” *J. Mater. Chem.*, vol. 17, no. 38, p. 3980, 2007.

[108] C. P. Klein, K. de Groot, A. A. Driessen, and H. B. van der Lubbe, “Interaction of biodegradable beta-whitlockite ceramics with bone tissue: an in vivo study.,” *Biomaterials*, vol. 6, no. 3, pp. 189–92, May 1985.

[109] S. Sarda, E. Fernandez, M. Nilsson, M. Balcells, and J. A. Planell, “Kinetic study of citric acid influence on calcium phosphate bone cements as water-reducing agent,” *J. Biomed. Mater. Res.*, vol. 61, no. 4, pp. 653–659, Sep. 2002.

[110] F. T. Mariño, J. Torres, M. Hamdan, C. R. Rodríguez, and E. L. Cabarcos, “Advantages of using glycolic acid as a retardant in a brushite forming cement,” *J. Biomed. Mater. Res. - Part B Appl. Biomater.*, vol. 83, no. 2, pp. 571–579, Nov. 2007.

[111] J. S. Román, B. Vázquez Lasa, M. R. Aguilar, and L. F. Boesel, “Modifications of bone cements,” in *Orthopaedic Bone Cements*, 2008, pp. 332–357.

[112] B. Ben-nissan, *Advances in Calcium Phosphate Biomaterials*, vol. 2, no. June 2016. Berlin, Heidelberg: Springer Berlin Heidelberg, 2014.

[113] D. Apelt *et al.*, “In vivo behavior of three different injectable hydraulic calcium phosphate cements,” *Biomaterials*, vol. 25, no. 7–8, pp. 1439–1451, 2004.

[114] E. Fernández, M. G. Boltong, M. P. Ginebra, O. Bermúdez, F. C. M. Driessens, and J. A. Planell, “Common ion effect on some calcium phosphate cements,” *Clin. Mater.*, vol. 16, no. 2, pp. 99–103, Jan. 1994.

[115] S. V. Dorozhkin, “Amorphous calcium (ortho)phosphates,” *Acta Biomater.*, vol. 6, no. 12, pp. 4457–4475, Mar. 2010.

[116] M. Bohner, U. Gbureck, and J. E. Barralet, “Technological issues for the development of more efficient calcium phosphate bone cements: A critical assessment,” *Biomaterials*, vol. 26, no. 33. pp. 6423–6429, Nov-2005.

[117] M. Shahrezaei, J. Shahrouzi, S. Hesaraki, and A. Zamanian, “α-Tricalcium Phosphate Effect on the Properties of Calcium Phosphate Bone Cements,” *J. Arch. Mil. Med.*, vol. 2, no. 2, pp. 1–7, 2014.

[118] J. Zhang, W. Liu, V. Schnitzler, F. Tancret, and J. M. Bouler, “Calcium phosphate cements for bone substitution: Chemistry, handling and mechanical properties,” *Acta Biomaterialia*, vol. 10, no. 3. pp. 1035–1049, Mar-2014.

[119] M. P. Ginebra *et al.*, “Setting Reaction and Hardening of an Apatitic Calcium Phosphate Cement,” *J. Dent. Res.*, vol. 76, no. 4, pp. 905–912, Apr. 1997.

[120] M. Komath, H. K. Varma, and R. Sivakumar, “On the development of an apatitic calcium phosphate bone cement,” *Bull. Mater. Sci.*, vol. 23, no. 2, pp. 135–140, Apr. 2000.

[121] M. Ikenaga, P. Hardouin, J. Lema??tre, H. Andrianjatovo, and B. Flautre, “Biomechanical characterization of a biodegradable calcium phosphate hydraulic cement: A comparison with porous biphasic calcium phosphate ceramics,” *J. Biomed. Mater. Res.*, vol. 40, no. 1, pp. 139–144, Apr. 1998.

[122] A. J. Ambard and L. Mueninghoff, “Calcium phosphate cement: Review of mechanical and biological properties,” *Journal of Prosthodontics*, vol. 15, no. 5. pp. 321–328, Sep-2006.

[123] S. Laasri, M. Taha, A. Hajjaji, A. Laghzizil, and E. K. Hlil, “Mechanical properties of calcium phosphate biomaterials,” *Mol. Cryst. Liq. Cryst.*, vol. 628, no. 1, pp. 198–203, Mar. 2016.

[124] P. Miranda, A. Pajares, E. Saiz, A. P. Tomsia, and F. Guiberteau, “Mechanical properties of calcium phosphate scaffolds fabricated by robocasting,” *J. Biomed. Mater. Res. - Part A*, vol. 85, no. 1, pp. 218–227, Apr. 2008.

[125] R. A. Perez, H.-W. Kim, and M.-P. Ginebra, “Polymeric additives to enhance the functional properties of calcium phosphate cements,” *J. Tissue Eng.*, vol. 3, no. 1, p. 20, Dec. 2012.

[126] T. Ogasawara, T. Sawamura, H. Maeda, A. Obata, H. Hirata, and T. Kasuga, “Enhancing the mechanical properties of calcium phosphate cements using short-length polyhydroxyalkanoate fibers,” *J. Ceram. Soc. Japan*, vol. 124, no. 2, pp. 180–183, Feb. 2016.

[127] D. S. Brazete, “Cimentos ósseos injetáveis à base de b-TCP,” Universidade de Aveiro, 2016.

[128] O. Bermúdez, M. G. Boltong, F. C. M. Driessens, and J. A. Planell, “Development of an octocalcium phosphate cement,” *J. Mater. Sci. Mater. Med.*, vol. 5, no. 3, pp. 144–146, Mar. 1994.

[129] O. Bermúdez, M. G. Boltong, F. C. M. Driessens, and J. A. Planell, “Optimization of a calcium orthophosphate cement formulation occurring in the combination of monocalcium phosphate monohydrate with calcium oxide,” *J. Mater. Sci. Mater. Med.*, vol. 5, no. 2, pp. 67–71, Feb. 1994.

[130] G. Limestone, T. Mountains, and W. Carpathians, “Calcium Phosphate Cements,” *Monogr. Oral Sci.*, vol. 18, no. 3, pp. 143–155, 2001.

[131] M. Bohner, H. P. Merkle, and J. Lemaître, “In vitro aging of a calcium phosphate cement,” *J. Mater. Sci. Mater. Med.*, vol. 11, no. 3, pp. 155–162, Mar. 2000.

[132] I. Ajaxon *et al.*, "Elastic properties and strain-to-crack-initiation of calcium phosphate bone cements: Revelations of a high-resolution measurement technique," *J. Mech. Behav. Biomed. Mater.*, vol. 74, pp. 428–437, 2017.

[133] I. Ajaxon and C. Persson, "Mechanical Properties of Brushite Calcium Phosphate Cements," 2017, pp. 285–300.

[134] J. Luo, I. Ajaxon, M. P. Ginebra, H. Engqvist, and C. Persson, "Compressive, diametral tensile and biaxial flexural strength of cutting-edge calcium phosphate cements," *J. Mech. Behav. Biomed. Mater.*, vol. 60, pp. 617–627, Jul. 2016.

[135] M. P. Ginebra, F. C. M. Driessens, and J. A. Planell, "Effect of the particle size on the micro and nanostructural features of a calcium phosphate cement: A kinetic analysis," *Biomaterials*, vol. 25, no. 17, pp. 3453–3462, Aug. 2004.

[136] H. Giesche, "Mercury porosimetry: A general (practical) overview," in *Particle and Particle Systems Characterization*, 2006, vol. 23, no. 1, pp. 9–19.

[137] J. Riikonen, J. Salonen, and V. P. Lehto, "Utilising thermoporometry to obtain new insights into nanostructured materials: Review part 1," in *Journal of Thermal Analysis and Calorimetry*, 2011, vol. 105, no. 3, pp. 1811–1821.

[138] D. Pastorino, C. Canal, and M.-P. Ginebra, "Multiple characterization study on porosity and pore structure of calcium phosphate cements," *Acta Biomater.*, vol. 28, pp. 205–214, Dec. 2015.

[139] A. Jillavenkatesa and R. A. Condrate, "The Infrared and Raman Spectra of β-and α-Tricalcium Phosphate ($Ca_3(PO_4)_2$)," *Spectrosc. Lett.*, vol. 31, no. 8, pp. 1619–1634, Dec. 1998.

[140] S. Pina, S. M. Olhero, S. Gheduzzi, A. W. Miles, and J. M. F. Ferreira, "Influence of setting liquid composition and liquid-to-powder ratio on properties of a Mg-substituted calcium phosphate cement," *Acta Biomater.*, vol. 5, no. 4, pp. 1233–1240, May 2009.

[141] E. Veiga, "Desenvolvimento de microagulhas de cimentos ósseos para libertação controlada de fármacos," Universidade de Aveiro, 2016.

[142] G. Mestres *et al.*, "Changes in the drug release pattern of fresh and set simvastatin-

loaded brushite cement," *Mater. Sci. Eng. C*, vol. 58, pp. 88–96, Jan. 2016.

[143] Z. Yang, J. Han, J. Li, X. Li, Z. Li, and S. Li, "Incorporation of methotrexate in calcium phosphate cement: behavior and release in vitro and in vivo.," *Orthopedics*, vol. 32, no. 107, p. 27, Jan. 2009.

[144] D. Samaha, R. Shehayeb, and S. Kyriacos, "Modeling and comparison of dissolution profiles of diltiazem modified-release formulations," *Dissolution Technol.*, vol. 16, no. 2, pp. 41–46, May 2009.

[145] G. Frutos, J. Y. Pastor, N. Martínez, M. R. Virto, and S. Torrado, "Influence of lactose addition to gentamicin-loaded acrylic bone cement on the kinetics of release of the antibiotic and the cement properties," *Acta Biomater.*, vol. 6, no. 3, pp. 804–811, Mar. 2010.

[146] A. C. Matos, L. M. Gonçalves, P. Rijo, M. A. Vaz, A. J. Almeida, and A. F. Bettencourt, "A novel modified acrylic bone cement matrix. A step forward on antibiotic delivery against multiresistant bacteria responsible for prosthetic joint infections," *Mater. Sci. Eng. C*, vol. 38, no. 1, pp. 218–226, May 2014.

[147] A. C. Matos *et al.*, "Novel doped calcium phosphate-PMMA bone cement composites as levofloxacin delivery systems," *Int. J. Pharm.*, vol. 490, no. 1–2, pp. 200–208, Jul. 2015.

[148] L. Yang *et al.*, "SERS investigation and detection of levofloxacin drug molecules on semiconductor TiO_2: Charge transfer contribution," *Colloids Surfaces A Physicochem. Eng. Asp.*, vol. 508, pp. 142–149, Nov. 2016.

[149] I. J. Hidi, M. Jahn, K. Weber, D. Cialla-May, and J. Popp, "Droplet based microfluidics: spectroscopic characterization of levofloxacin and its SERS detection.," *Phys. Chem. Chem. Phys.*, vol. 17, no. 33, pp. 21236–42, Aug. 2015.

[150] P. V Riboud, "Composition et stabilité des phases a structure d'apatite dans le système CaO–P_2O_5–oxyde de fer–H_2O à haute température," *Ann. Chim*, vol. 8, no. 8, pp. 381–390, 1973.